Using an accelerated aging model and an optimised proteomic approach to identify extracellular vesicle-associated proteins in inflammaging

Nicolas Lafrenière

A thesis submitted to the University of Ottawa
in the partial fulfillment of the requirements for the
Master of Science in Biochemistry degree

Department of Biochemistry, Microbiology, and Immunology
Faculty of Medicine
University of Ottawa

ABSTRACT

Senescent cells contribute to inflammaging through the senescence-associated secretory phenotype (SASP). While the SASP has traditionally been identified by the release of soluble protein factors such as cytokines, extracellular vesicles (EVs) have recently emerged as important components of the SASP due to their cargo of diverse bioactive molecules. Individuals with early or accelerated aging often exhibit an increased burden of senescent cells. Hutchinson-Gilford Progeria Syndrome (HGPS), a rare and fatal genetic disorder, serves as a valuable model for studying accelerated biological aging and has played a pivotal role in elucidating SASP mechanisms. However, the composition and functional roles of EVs in HGPS remain poorly understood.

In this study, we optimized a workflow for isolating and characterizing EVs from HGPS fibroblasts cultured *in vitro*. Using liquid chromatography–tandem mass spectrometry (LC-MS/MS) in the data independent acquisition (DIA) mode, we identified over 1,500 unique proteins in EVs secreted by both HGPS and age-matched healthy control fibroblasts. Among these, we observed significant dysregulation of Major Histocompatibility Complex I (MHC-I) Human Leukocyte Antigen C (HLA-C) in EVs derived from mixed populations of replicating and senescent HGPS fibroblasts, compared to healthy controls. Notably, LNPEP (also known as IRAP), a protein involved in MHC-I antigen loading in endosomes, was upregulated in HGPS fibroblasts. CD9, a canonical EV marker implicated in inflammatory signaling was also upregulated in HGPS-derived EVs.

These findings suggest that EVs may participate in modulating immune responses to senescent cells, potentially contributing to the impaired clearance of senescent cells observed in age-related diseases. Our study provides novel insights into the EV-mediated component of the SASP in HGPS and underscores the broader relevance of EVs in diseases characterized by accelerated aging and cellular senescence.

ACKNOWLEDGEMENT

I would first like to thank Dr. Arsalan Haqqani for giving me the opportunity to take charge and work on this project under his guidance, while personally teaching me the ins and outs of mass spectrometry. Never would I have imagined getting the opportunity to work at the National Research Council, and it was truly an honour to be your first "official" graduate student after you got adjunct professorship. I would also like to thank Dr. Dylan Burger for accepting to be my co-supervisor, for his insights into EV biology and for being my greatest link to the university. Last, but not least, I would like to thank Dr. Jagdeep K. Sandhu for accepting to supervise me as an undergraduate TMM honours student and as a master's student, success in both projects would have been impossible without your vast expertise in immunology and dedication to your students. I cannot think of a time where we interacted, and I have not learned something. I thank you all for the opportunity to further my studies. I would also like to thank my thesis advisory committee members, Dr.Carolina Ilkow and Dr. Derrick Gibbings, who have helped broaden my horizons in this project and for their sage advice during this accelerated program.

Many people have contributed directly and have supported this project with their technical expertise. I thank Dr. Fengxia Xiao of the Ottawa Hospital Research Institute for producing the biological materials delivered to the National Research Council that were needed as the basis of this project, along with Agafe Reyes and Syndey Pitre who have assisted in Fengxia's absence. I would like to thank the Bioanalysis team at NRC, notably Alexandra Star, Wen Ding, Samiksha Vij; and Anna Robotham, Tammy-Lynn Tremblay, Dr. Jennifer Hill and Bianca Dupont of MS & NMR Analytics for their insightful conversations. The NRC Analytics Facility, Luc Tessier, Sam Williamson, Ken Chan and Jean Kan always kept the mass spectrometers in good working order for whatever experiment I needed to run, for which I am grateful. Finally, I would like to thank the NRC Preclinical Imaging team composed of Melissa Hewitt, Klaudia Baumann, Dr. Christine

Péladeau-Ladouceur and Dylan Layton-Matthews for their support with the in vitro experiments at the Montreal Road National Research Council Campus. While any omissions are unintentional, I truly do appreciate the assistance from everyone involved, no matter how indirectly, to this project.

I would not have gotten this far in my education if not for the love and support of my family, my parents, and brother Mathieu.

I dedicate this thesis to my parents, Lisa and Norm, who have always supported my endeavours and were always ready to act as a sounding board for my wild ideas, even when they had no clue about what I was saying.

STATEMENT OF CONTRIBUTIONS

The work, analyses and writing presented in this thesis was entirely performed by the student, Nicolas Lafrenière (NL), unless otherwise noted below.

Cell culture of HGPS and Healthy fibroblasts, conditioned media collection from these cells and initial media concentration was performed by Dr. Fengxia Xiao (FX), Agafe Bless Reyes (ABR) and Cydney Pitre (CP) of Dr. Dylan Burger (DB) Lab. Conditioned media concentration methods were refined by NL.

Mass spectrometric methods used (liquid chromatography and mass spectrometer instrument settings) were developed by Dr. Arsalan Haqqani (ASH), Alexandra Star (AS) of National Research Council Canada (NRC). PRM-EV51 method, to assess EV markers by mass spectrometry was developed by AS and refined as needed by NL. All other PRM methods were developed by NL. Mass spectrometer qualification and system suitability testing was performed by the NRC Analytics Facility. NL developed the project-specific quality control method.

Conceptualization of experiments was performed jointly by ASH, DB, JKS, NL.

Funding

The work presented herein was funded by a National Research Council New Beginnings Ideation Fund (2023-2024) grant held jointly by ASH and DB. Further funding was obtained by DB via an NSERC Discovery Grant (RGPIN-2021-03424). NL acknowledged a National Research Council Studentship during the summer of 2024 from funding derived from ASH's New Beginning's grant.

TABLE OF CONTENTS

LIST OF ABBREVIATIONS

AIM2	Absent in Melanoma 2
AF4	Asymmetric-flow field-flow fractionation
ALIX	ALG-2-interacting protein X (see PDCD6IP)
AMBIC	Ammonium Bicarbonate
ANOVA	Analysis of Variance
ATP	Adenosine Triphosphate
β2M	β-2-microglobulin
BSA	Bovine Serum Albumin
Ca^{2+}	Calcium
CD8	Cluster of Differentiation 8
CD27	Cluster of Differentiation 27
CD28	Cluster of Differentiation 28
CD57	Cluster of Differentiation 57
CD63	Cluster of Differentiation 63
CD81	Cluster of Differentiation 81
CDK	Cyclin-dependent Kinase
CDKN1A	Cyclin-dependent Kinase Inhibitor 1A
CDKN2A	Cyclin-dependent Kinase Inhibitor 2A
CM	Conditioned Media
COPD	Chronic Obstructive Pulmonary Disease
COVID-19	Coronavirus Disease 2019
CRP	C-reactive Protein
Da	Dalton
DDA	Data Dependent Acquisition
DIA	Data Independent Acquisition
DNA	Deoxyribonucleic Acid
DSB	Double Stranded Break
dsDNA	Double-stranded DNA
DTT	Dithiothreitol
ELISA	Enzyme Linked Immunosorbent Assay
EMEM	Minimum Essential Medium Eagle
EP	Extracellular Particle
ESCRT	Endosomal Sorting Complex Required for Transport
EV	Extracellular Vesicle
FBS	Fetal Bovine Serum
FTI	Farnesyltransferase Inhibitor
GLB1	β-Galactosidase 1
GSN	Gelsolin
GST	Glutathione S-transferase
GSTO1	Glutathione S-transferase Omega 1
HC	Healthy Control
HGPS	Hutchinson-Gilford Progeria Syndrome
HLA	Human Leukocyte Antigen
HMGB1	High-mobility Group Box 1
IAA	Iodoacetamide

IL-1β	Interleukin 1β
IL-6	Interleukin 6
IL-18	Interleukin 18
ILV	Intraluminal Vesicle
ISG	Interferon Stimulated Genes
LC	Liquid Chromatography
LC-MS/MS	Liquid Chromatography Tandem Mass Spectrometry
LDHA	Lactate Dehydrogenase A
LDHB	Lactate Dehydrogenase B
LFQ-MBR	Label-Free Quantification Match Between Runs
LMNA	Lamin A
LMNB1	Lamin B1
LPS	Lipopolysaccharide
MAM	Mitochondrial-associated Membrane
MHC-I	Major Histocompatibility Complex Class I
miR	Micro-RNA
MISEV	Minimal Information for the Study of Extracellular Vesicles
MV	Microvesicle
MVB	Multivesicular Body
m/z	Mass-to-charge ratio
NEK7	NIMA Related Kinase 7
NK	Natural Killer (lymphocytes)
NKG2D	Natural Killer Group 2 Member D
NLRP3	NOD-, LRR-,and Pyrin Domain-containing Protein 3
NTA	Nanoparticle Tracking Analysis
NVEP	Non-Vesicular Extracellular Particle
PDCD6IP	Programmed Cell Death 6-interacting Protein (see ALIX)
PBS	Phosphate-buffered Saline
PCV	Purified Collection Volume
PMA	Phorbol 12-myristate-13-acetate
PPI	Protein-protein Interaction
PRM	Parallel Reaction Monitoring
PTM	Post-translational Modification
ROS	Reactive Oxygen Species
RNA	Ribonucleic Acid
RNS	Reactive Nitrogen Species
SA-β-Gal	Senescence Associated β-galactosidase (staining)
SASP	Senescence-Associated Secretory Phenotype
SDS	Sodium Dodecyl Sulfate
SEC	Size Exclusion Chromatography
sEV	Small Extracellular Vesicle
SERPIN	Serine Protease Inhibitor
SOD	Superoxide Dismutase
SP3	Single-Pot Solid-Phase Enhanced Sample Preparation
TNFα	Tumor Necrosis Factor α
UC	Ultracentrifugation

UF	Ultrafiltration
UF-SEC	Ultrafiltration-Size Exclusion Chromatography
UN	United Nations
WCL	Whole Cell Lysate

LIST OF FIGURES

LIST OF SUPPLEMENTAL FIGURES

LIST OF TABLES

LIST OF SUPPLEMENTAL TABLES

1. INTRODUCTION

1.1. Aging

1.1.1. Clinical and Societal Impacts of Aging

The Canadian and global populations are rapidly aging, which poses threats to healthcare systems worldwide as older adults often have complex health needs[1]. The United Nations (UN) project that the number of older adults, those being greater than the age of 65, will increase from 10% in 2021 to 16% by 2050 (Figure 1A) [2]. Other projections for the year 2100 suggest 124 nations around the world will be super-aged societies, where at least 20% of the population is over the age of 65 [3]. Canada is expected to become super-aged by 2030 (Figure 1B), thus an important proportion of the population will be geriatric. This worldwide increase in lifespan has been considered a "major human achievement" by the UN, fueled by scientific inquiry into novel medicines, as no significant proportion of any recorded population worldwide had attained that milestone per data from the 1950s [4]. This achievement is also further exemplified when comparing the modern human lifespan to that of other Great Apes, whose lifespan rarely exceeds 50 years in captive environments[5].

A second key measure is also used to understand the aging population, that being healthspan or health-adjusted life expectancy, which is defined by many as the length of time people live before being affected by significant disease or disability which is associated with aging[6,7]. Some researchers caution the use of this term, until such a time where a "significant disease" is comprehensively defined across different societies and cultures[6]. However, others conjecture this metric of longevity is currently useful, to quantify healthy aging in current times, and measure its evolution moving forward[8]. Of particular interest is the "healthspan gap" or "longevity leap", the difference between lifespan and healthspan, which sits approximately between one seventh and one fifth of lifespan (Figure 1C) [3,9]. Thus, people will live up to 20% of their life with some

advanced degree of disease. Upon further investigation of two-decades of global data, while excluding communicable disease and the year's corresponding to the coronavirus disease 2019 (COVID-19) pandemic, it was found that women and individuals from developed countries display a larger average healthspan gap when compared to the global mean, the underlying reasons for this is still poorly understood[7].

In recent years, the UN has declared a "Decade of Healthy Aging", a framework to promote the evolution of the social views of longevity towards healthy longevity[10]. Though, this did not explicitly include scientific inquiry into the biological underpinnings of the healthspan gap, it is interesting to note that countries which display the largest gap tend to be westernized, and harbour an increased burden of sterile inflammation driven, in part, by noxious metabolic stimuli arising from western diets amongst other sources, termed meta-inflammation[11,12]. This metabolic inflammation is distinct from inflammaging, but a complex crosstalk has been identified between the two in the context of many diseases which increase in frequency and severity with age, known as age-related diseases[13,14].

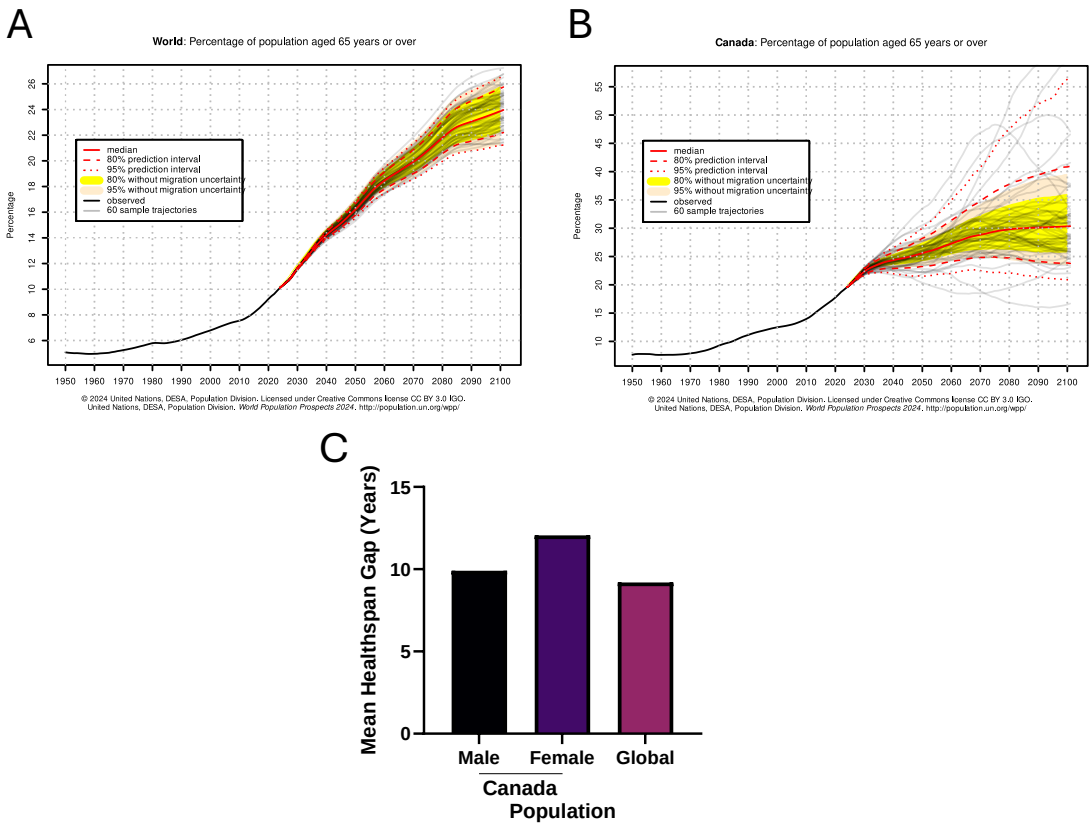

Figure 1: A Global and Canadian perspective on aging.

(A) Proportion of the global population of age 65 or older, from 1950 and projected to 2100. **(B)** Proportion of the Canadian population of age 65 or older, from 1950 and projected to 2100. **(C)** The mean healthspan gap of Canadians stratified by sex, and the global mean healthspan gap. Panels (A) and (B) were used from the United Nations, under the Creative Commons License CC BY 3.0. Data for panel (C) come from analyses performed by Garmany and Terzic, 2024 [9].

1.1.2. Inflammaging: The Intersection of Inflammation and Aging

It is well understood that important contributing factors to reduced healthspan are pathologies such as cancer, cardiovascular disease, dementia, diabetes and neurodegenerative disease, all of which are becoming increasingly prevalent in modern society[3,15]. Together, these are all age-related disorders, of which a major risk factor is inflammaging, a term first coined in 2000 in the context of evolutionary biology and medicine[16,17]. Its definition has matured over the past two and a half decades, but it is currently defined as the increase in sterile inflammation with advancing chronological age[18]. As there is no overt infection and inflammatory response, some refer to this inflammation as "smoldering" and is still capable of having profound pathological implications[19]. Despite the reuniting risk factors for age-related diseases, aging itself is exceptionally heterogenous in onset, rate and progression, even within the same organism; certain populations also display premature aging[20–23]. Therefore, an understanding of the inflammaging process is essential to develop novel interventional strategies to promote healthspan into older adulthood.

Inflammaging is characterized by the chronic activation of the innate immune system, such as an increased macrophage activity[24]. Serum levels of various pro-inflammatory mediators such interleukin 6 (IL-6), and tumour necrosis factor alpha (TNFα) along with other chemokines and cytokines are high when assessed by molecular and proteomic methods[25,26]. Elevated levels of these mediators trigger a chronic pro-inflammatory state in the body and facilitate the development or progression of many diseases[27,28]. A consequence of this long-term immunogenic state is immunosenescence, where cellular components of the immune system, both innate and adaptive, undergo senescence and cease normal function by permanently exiting the cell cycle, and reprogramming their metabolic phenotype[29]. The dysfunctional immune system of the elderly is partially responsible for the increased vulnerability to many infectious and auto-immune diseases[30].

The array of dysregulation which is observed in immunosenescence is large, however, important changes occur in Natural Killer (NK) and $CD8^+$ thymus (T) lymphocytes. NK cells, despite increasing in number as humans age, demonstrate decreased secretion of pro-inflammatory mediators when undergoing senescence, which is contrary to what is observed in virtually all other cell types[31–34]. This has been associated with decreased perforin expression and release via degranulation, a protein which is linked to NK cell killing efficiency[35–37]. Further investigation of NK cell degranulation using compounds such as phorbol 12-myristate 13-acetate (PMA) in aged samples suggests that the reduction of cytotoxicity lies within modifications to signaling pathways leading to degranulation from membrane receptors, as degranulation using PMA, which bypasses these receptors, doesn't differ between young and aged groups[38]. In studies involving mice, the host non-hematopoietic microenvironment was determined to be a key regulator of age-related decline in NK-cell cytotoxicity[39]. Thus, a complex interplay of cell-intrinsic and extrinsic factors is important in NK cell immunosenescence.

T cells have been extensively studied in the context of aging, particularly due to the thymic involution, or the gradual shrinking of the thymus gland with age which was first described by anatomists[40,41]. The changes observed in the thymus are accompanied by a concomitant decrease in mature T cells in peripheral tissues and the loss of diversity in the T cell repritoire[40,42]. In turn, this research focus has then highlighted the importance of T cell immunosenescence, as many cell-intrinsic changes occur in the decreased populations of T lymphocytes that remain. General observations include decreases in costimulatory molecules such as CD27 and CD28 which are essential in activated T cell survival and generation of effector T cell pools, and increase in CD57, which taken together suggest a replicative senescence[43,44]. Notably, this is distinct from T cell exhaustion, which is a reversible dysfunction, whereas T cell senescence is a terminal process, and

is accompanied by many changes which are well documented in somatic cells (see below in section 1.1.3)[45]. One of the greatest differences between the two T cell dysfunctions elaborated above is that T cell senescence is accompanied by an altered, pro-inflammatory secretome, which is in stark contrasts to the modifications seen in NK cell immunosenescence.

1.1.3. Cellular Aging and Senescence

Despite immunosenescence being an important driver of age-related disease, virtually all terminally differentiate cell types are capable of undergoing senescence in response to stress and damaging stimuli as illuded above. The most relevant triggers include nuclear instability, chromosomal damage, telomere erosion, epigenetic reprogramming and metabolic imbalances. In 2013, work published by López-Otín and colleagues grouped these factors together as "The Hallmarks of Aging", along with senescence[46]. In the most recent rendition of these hallmarks, chronic inflammation was added to this list as it is the result of all other hallmarks, while also providing a powerful feedforward mechanism to induce further derangement to cellular function associated with advanced age [47].

The senescence that was first described by Hayflick and Moorhead over 60 years ago occurred by the serial passaging of human cells, which was termed replicative senescence and was causally linked to telomere attrition upstream of chromosomal instability[48,49]. Cellular senescence is associated with the permanent exit from the cell cycle; however, these cells persist and function with an altered metabolic profile, such as the senescence associated secretory phenotype (SASP). In pathological contexts, the increase in oncogene Ras can lead to oncogene-induced senescence, producing DNA damage via double stranded DNA breaks (DSB)[50]. Other stressors which lead to DNA lesions, such as reactive oxygen species (ROS) may promote stress-induced, often referred to as premature, senescence[51]. Despite these various signals to begin the senescence program, DNA repair processes are of prime importance while sets of conserved pathways, such as p53,

allow for the progression of cellular senescence. Under physiological conditions, p53 (also known as TP53) is consistently produced and promptly degraded following its ubiquitination by MDM2, acting within an autoregulatory feedback loop as the MDM2 gene contains a p53 DNA-binding site[52]. However, in response to DNA lesions, repression of p53 is halted by phosphorylation, and by checkpoint serine/threonine kinases CHK1 and CHK2, which are activated by master transducers of DNA damage ATM and ATR[53].

When a cell becomes senescent, it is arrested in the cell cycle oftentimes due to the upregulation and activation of cyclin dependant kinase (CDK) inhibitors which target key regulatory steps of the cell cycle, notably CDKN1A (p21) and CDKN2A ($p16^{INK4a}$). In some cases, this may be the result of nuclear instability caused by decreases in Lamin B1 (LNMB1), High Mobility Group Box 1 (HMGB1) or other protein components of the nuclear lamina, envelope and DNA scaffolds[54,55]. However, a nucleus-centric view doesn't fully capture the breadth of dysregulation that may occur to induce senescence, rather, defective organellar quality control mechanism such as autophagy and mitophagy, fuel important metabolic changes within senescence cells[56]. Furthermore, distinct sites of recycling such as the proteasome undergo pathological changes and concomitant increases in lysosomal mass and β-galactosidase (GLB1), a glycoside hydrolase with effects on β-galactosides within the lysosomal compartment[57–59]. Separately and together, these changes are important derangements within senescent cells.

Cellular dysfunction is not only limited to the intracellular spaces; senescent cells display an array of immunogenic features known as the SASP[60]. The initial description of this phenotype was somewhat limited using antibody-arrays at the time, it is now appreciated as a heterogenous secretome. Cells of myeloid and other lineages secrete high levels of pro-inflammatory mediators such as cytokines, chemokines, ROS, reactive nitrogen species (RNS), extracellular proteins,

proteases and C-reactive protein (clinically relevant as CRP). The precise makeup of the SASP varies depending on the lineage of the senescent cell and nature of damage the cells were subject to which led to senescence[61]. Within the past few years, extracellular vesicles (EVs) have been added to the SASP as an insoluble component with the ability to spread inflammageing and senescence to nearby and distant cells via the immune-silent transport of pro-geronic factors[62,63]. EVs have also been found to interact with and stabilise various factors of the soluble SASP, such as cytokines[64].

The effects of the increased burden of senescent cells with advanced age has been an area of active inquiry, as the increase in senescent cell numbers have deleterious effects on tissues and organs[65]. The body has natural mechanisms in place to regulate the accumulation of senescent cells and minimize their negative effects on the organism. The SASP, being pro-inflammatory is a potent chemo-attractant of the innate immune system, notably macrophages, T and NK lymphocytes[66], thereby increasing immunosurveillance of cells expressing the senescent program. However, as the SASP is an important player in tissue microenvironments, it may be relevant to the decrease in NK cell cytotoxicity observed in aging[67].

The innate immune response to senescence cells after SASP production generally entails the recruitment of M1-like macrophages, which are mainly involved in pro-inflammatory responses whereas M2-like macrophages are mainly involved in anti-inflammatory responses. Next, NK cells are recruited to the site and bind to the senescent cells via NKG2D ligands, where NK-cell derived perforins and granzymes are used to clear the senescent cells[66]. However, expression of major histocompatibility complex I (MHC-I) human leukocyte antigen (HLA) proteins are important inhibitors of NK cell activity. Upregulation of HLA-E has been found to inhibit NK and CD8+ (effector) T cell clearance of the senescent cells, while it's depletion increased CD8+ T cell-

mediated killing [68]. There has been no other inquiry into the roles of other HLA paralogs in senescent cell clearance.

Despite the current description of senescence presented above focuses primarily on the negative aspects of the process, it would be inappropriate to ignore the key roles of senescence in developmental biology, and tissue repair. Developmental senescence was found to be similar to oncogene-induced senescence, where p21 was found to be highly expressed with little to no expression of p53 in mouse embryos[69]. Evidence of senescence was also observed in human embryonic development[70]. In mice, selective removal of senescent cells inhibited wound healing; exogenous addition of certain SASP factors reversed this effect[71]. In human cutaneous wound healing, p21 and p53 were found to be upregulated amongst other senescence markers[72]. Despite this evidence and an acknowledgement that senescence is not strictly pathological, this thesis will assess senescence through the classical pathological lens, which is particularly notable in the case of progeroid diseases.

1.2. Progeroid Syndromes – Diseases of Aging

Progeroid syndromes are a class of rare genetic diseases characterized by their high degree of similarities to the physiological aging process, at exceptionally early stages of life. Some of these diseases include Bloom syndrome, Cockayne syndrome and Werner syndrome[73]. Hutchinson-Gilford Progeria syndrome (HGPS) is likely the most known of all the progerias and generally results in death by the age of 13 years[74]. Current therapeutic avenues are only life-extending with some regard for quality of life in those extended years, but ultimately non-curative[75,76]. In most cases, the causative mutation in HGPS is a spontaneous mutation (c.1824C>T) in exon 11 of the Lamin A (LMNA) gene, leading to improper post-translational processing and the retention of a farnesyl modification on the mature protein[77,78]. In these patients, the matured form of the mutant LMNA pre-protein is therefore called “progerin” due to the protein’s association with the induction

of a premature aging phenotype[78]. The progerin isoform retains its ability to be a nuclear lamina protein but causes nuclear instability and is associated with various chromosomal effects[79]. Base-editor technology has been implemented in mouse models of HGPS carrying mutant LMNA, to greatly extend lifespan; however, no translatory efforts have been successful to date[80].

HGPS patients are afflicted with co-morbidities such as hypertension and atherosclerotic cardiovascular disease leading to stroke, myocardial infarction and cardiac failure; all this without classical risk factors for these morbidities such as smoking and obesity[74]. Signs and symptoms of HGPS include the loss of subcutaneous fat, muscle atrophy, osteopenia, joint stiffness and progressive alopecia[81]. Together, these observations demonstrate that HGPS is indeed a disease which mimics physiological old age; thus, it has been used as a model system to understand the aging process and develop better therapeutics[82,83].

The most common HGPS samples used for *in vitro* biomedical research are dermal fibroblasts. Fibroblasts are important mesenchymal cells of connective tissues that secrete extracellular matrix and signalling molecules such as cytokines and growth factors, among other roles in signal transduction[84]. However, due to the presence of this cell in many diverse tissues, fibroblasts exhibit great functional and transcriptional heterogeneity. These cells are increasingly recognized for their ability to shape microenvironments within the body, particularly under disease conditions[85]. Seminal work to understand HGPS immunology and inflammaging has also occurred using lymphoblasts, though, these cells are still used relatively rarely when compared to their fibroblast counterparts[86].

The NLRP3 inflammasome, the most promiscuous of cytosolic sensors for danger associated molecular patterns and a central mediator of inflammation, has been shown to be activated in lymphoblasts from HGPS patients[86]. Furthermore, the components of the NLRP3 inflammasome

were also activated in a mouse model (Zmpste24$^{-/-}$) of HGPS and pharmacological inhibition of NLRP3 inflammasome by a small-molecule drug, MCC950, improved the lifespan of these mice and reduced IL-1β production[86,87]. These findings suggests that NLRP3-inflammasome dependent inflammation might be linked to the increase and promotion of inflammaging in HGPS and old age. Therefore HGPS remains an attractive model system to study the SASP[88].

An important nexus for NLRP3 inflammasome activation is the mitochondria and mitochondrial associated membranes (MAMs), which are contact sites between the mitochondria and endoplasmic reticulum. When innate immune cells, such as macrophages and microglia are exposed to ER stressors, the flux of calcium (Ca^{2+}) into the mitochondria may lead increases in mitochondrial oxidative stress and superoxide dismutase (SOD2) upregulation[89]. Another important class of antioxidants are glutathione S-transferases (GST) enzymes, which transfer glutathione tripeptides onto electrophilic species, while also serving as important components of the global protein glutathionylation system. In the context of the NLRP3 inflammasome, GST Omega-1 (GSTO1) has been identified as an important positive regulator of the inflammasome via deglutathionylation of NIMA related kinase 7 (NEK7)[90]. Although, these specific antioxidants and their connection to inflammation in HGPS has never been fully examined, dietary magnesium has been found to ameliorate mitochondrial oxidative stress in heterozygotic LMNA mutant mice and ultimately lead to improved lifespan[91]. In other preclinical models, compounds with antioxidant properties such as methylene blue or RAD001 (Everolimus, rapamycin analog)[92,93]. As RAD001 has been already approved for clinical use in cancer, a new trial involving laminopathy patients has been launched, however, no results have been published at the time of writing this thesis[93,94].

Farnesyltransferase inhibitors (FTIs) are a class of drugs that were first developed to treat cancers, specifically in cancers where there are mutations in the RAS family of proteins which

require farnesylation to become functional at the cell membrane and exert their pro-proliferative effects[95]. For example, Lonafarnib (also known as SCH66336, Sarasar and Zokinvy), was initially used in multiple cancers, but had a small proportion of patients who responded to the molecule as a monotherapy or combination therapy, potentially due to the alternative prenylations other than farnesylation which may occur to mutated RAS[96–98]. However, in 2020, Lonafarnib was approved by the Food and Drug Administration for the treatment of HGPS, with its therapeutic effect acting through the inhibition of farnesylation of preprogein[99].

Due to the wide array of pathological observations in HGPS, many other cellular pathways and processes may be promising as targets for disease-modifying therapies, or solutions which work beyond symptom management such as antioxidant therapies. Telomere length is shorter in HGPS when compared to health, chronological age-matched controls, thus targeting telomere attrition mechanisms may be useful[100]. Indeed, efforts have been made in telomere-driven diseases, such as aplastic anemia, to inhibit the attrition or increase telomere length through telomerase activity. Supplementation with telomerase activator TA-65 has shown moderate success in telomere lengthening, without significant impacts on organism longevity[101]. Androgen therapy has demonstrated the potential to increase TERT transcription and rescue telomere attrition; however, this therapeutic approach presents the largest benefit in hematological cell types[102]. The relative lack of research in the HGPS immune system may limit the utility of these approaches to the disease.

1.3. Extracellular Bioparticles and Vesicles

Extracellular vesicles (EVs) are submicron, lipid bilayer-bound extracellular particles (EPs) that were first described as cellular debris or “platelet dust”, that are shed by all cell types and are readily accessible in many bodily biofluids such as blood and urine[103,104]. These particles are now appreciated as important mediators of paracrine and endocrine communication due to their rich

contents of nucleic acids, proteins and lipids; as well as their stability in circulation or extracellular environments, tropism and low immunogenicity. These factors have contributed to EVs becoming attractive targets for the identification of biomarkers or as highly customizable delivery vehicles for novel therapeutics.

Given the heterogeneity of EVs, they can be classified by biochemical composition, density, and size among other quantitative measures proposed in 2014, and revised twice since then, most recently in 2023[105–107]. A wide variety of molecular markers, such as proteins, lipids and micro-RNAs (miRs) exist for general and specific subclasses of EVs, indexed on databases such as Vesiclepedia and ExoCarta[108,109]. The most consistently described protein markers are tetraspanins such as CD63, CD81 and CD9, and antibody-based recognition of these proteins is feasible and often used. The Minimal Information for Studies of Extracellular Vesicles (MISEV) has, historically, curated a non-exhaustive list of proteins divided into categories, depending on protein topology, protein function, specific association with EVs, associations with contaminating co-isolated EPs or subcellular trafficking pathways and contaminants from the sample matrix or cell culture medium[107]. Along with this list of proteins, the MISEV Consortium has produced thorough guidelines with respect to all aspects of EV research and reporting. Size-based discrimination of EVs produce subcategories such as small EVs (sEVs), which are smaller than 200 nm in diameter, and large (lEVs) which are greater than 200 nm. The use of such size terms is cautioned by MISEV 2023, as these definitions are dependent on the technique of measurement used in a particular study while some techniques induce artefactual physical properties[107].

EV biogenesis pathways are varied, depending on the exact subpopulation in question. Exosomes, which are nanoparticles of size 30-120 nm, are generated from the late endosome[110]. Large multivesicular bodies (MVBs) allow for the formation of intraluminal vesicles (ILVs) by

invagination of late endosomal membranes, an event which may engulf and trap cytosolic components in a macroautophagic process[111]. The ILVs within the MVBs have two major fates, 1) the trafficking to the lysosome for cargo degradation or 2) the release of the ILVs into the extracellular space upon fusion with the plasma membrane. The extracellularly released ILVs are termed small extracellular vesicles or exosomes. Due to this biogenesis mechanism, exosomes typically contain the machinery known as the endosomal sorting complex required for transport (ESCRT); however, recent evidence suggests that an ESCRT-independent exosome biogenesis pathway which is dependent on lipid raft microdomains may also be important[112,113]. These domains have been shown to be enriched with tetraspanin, proteins which are widely accepted to be crucial in exosomal protein loading, forming tetraspanin enriched microdomains [114].

Microvesicles (MVs) are a distinct class of EVs, and larger than exosomes, being defined as 150-1,000 nm in diameter. These structures are sometimes referred to as microparticles. MVs are the product of direct outwards budding of the plasma membrane, rather than structure from within the cell that is then released, their upper size limit has an important dependence on their cell of origin. As the outwards membrane blebbing is accompanied by changes in protein and lipid composition, to facilitate membrane curvature required for MV formation[115]. Of note, MVs are a heterogenous group of structures, when applying the definition of being formed by the outwards blebbing of the plasma membrane, which encompasses subclassifications of EVs such as oncosomes and apoptotic bodies[116]. Both subclasses have specific requirements for their classification, particularly with respect to the producing cell, like cancer for oncosomes and cells undergoing apoptosis for apoptotic vesicles and bodies[117–119].

The most widely studies biochemical cargo of EVs are likely miRs, due to their potency at modulating biological processes via posttranscriptional actions[120,121]. In the context of senescence,

miR34a has been shown to promote the propagation of senescence by EVs in chronic obstructive pulmonary disease (COPD), a lung-specific premature aging pathology, by inhibiting the anti-aging protein surtuin-1 [122]. Senescent osteoblast-derived EVs were found to promote endothelial cell senescence through their miR-214-3p cargo, which targets L1CAM[123,124]. The transfer of miRs via exosomes also has clinical implications, such as miR-181b-5p mediated senescence in doxorubicin-resistant breast cancers[125]. The composition of the EV lipid envelope has been shown to change as well, though, the possible effects these changes have on target cells has yet to be determined[126]. The protein cargo of senescent cell EVs has also been demonstrated in many human cell models, such as vascular smooth muscle where the cargo induced pro-inflammatory effects on target immune cells which were consistent with inflammaging[127]. A recent review has summarized some of the changes in EV cargo and their effects on immunosenescence and inflammaging[128]. A schematic of the SASP, including the novel EV components is presented in Figure 2. In this study, I sought to examine the EV proteins that are disturbed in HGPS, a classically senescent cell and model of advanced chronological age, using mass spectrometric methods.

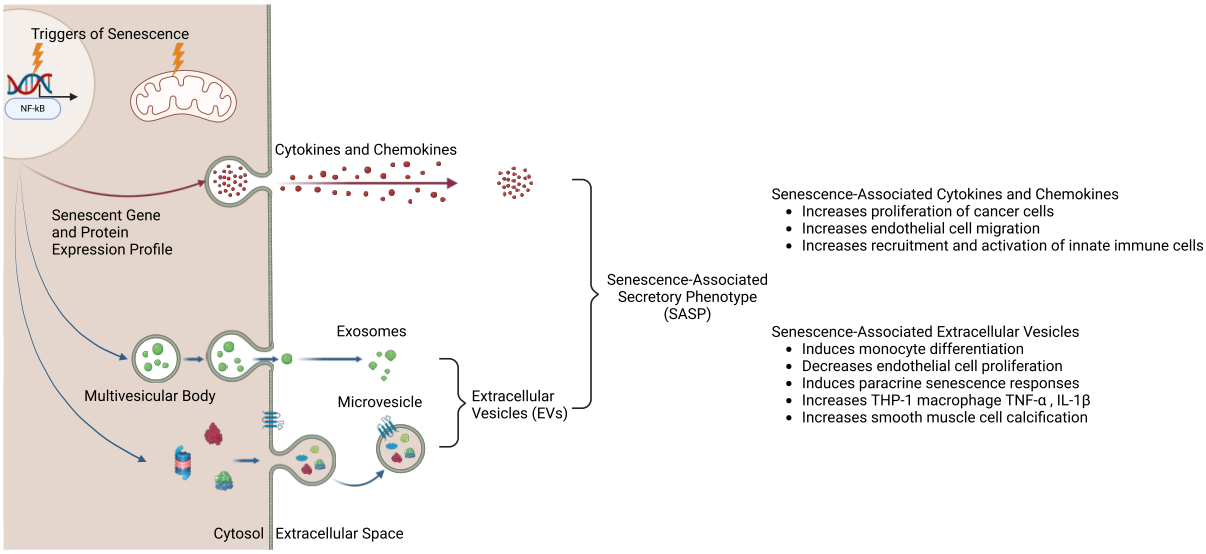

Figure 2: EVs as a component of SASP.

EVs are increasingly recognised as important mediators of the SASP. When a cell becomes senescent, due to a variety of triggers such as DNA damage or mitochondrial stress and dysfunction, a senescent gene expression profile is expressed, which classically included pro-inflammatory SASP markers. However, protein-level changes may also modify the non-soluble secretome, contained within various EV subpopulations such as exosomes or microvesicles. Both SASP compartments, either soluble or non-soluble, can induce a pro-inflammatory effect, such as immune cell activation. Despite EVs, being classically referred to as “immune silent”, in the context of the SASP, they represent an important feed-forward mechanism to promote inflammation in nearby and distant targets.

1.4. Mass spectrometry as a tool for molecular characterization

Proteins are the result of translated RNA and are key effectors of nearly all cellular processes. Thus, understanding these biomolecules is important to understand biological systems. Proteomics is the study of the protein landscape of biological samples, including protein expression, post-translational modifications (PTMs) and in some cases protein localization. With knowledge of the human genome, inferences may be made about the proteome for subsequent large-scale protein sequencing experiments. To date, the UniProt Consortium maintains a human reference proteome of over 20,000 proteins, representing full genomic coverage[129]. This tool, along with instrument development has allowed for unparalleled quantitative sequencing of protein and peptide data.

The current method for identifying hundreds or thousands of proteins in complex biological samples is bottom-up proteomics, whereby samples are digested with proteolytic enzymes cleaving known residues[130]. This peptide sample is then subject to liquid chromatography (LC) to separate peptides by their relative hydrophobicity and the eluted peptides are directly sprayed (via electrospray ionization) into mass spectrometer, which measures mass-to-charge (m/z) values of intact peptides (precursor ions), fragments the peptides, and measures m/z values of peptide fragments (fragment ions).

As the quality of the data collected is directly correlated with the proteins which may be identified in a mass spectrometry experiment, many distinct data acquisition methods have been developed to maximize reproducible protein identification. Notably, data dependent acquisition (DDA) selects a pre-defined number (N) of the most intense peaks in the precursor MS1 scan (i.e. peptides with specific charges) for fragmentation and more detailed analysis during the MS2 scan to produce a unique spectral “fingerprint” for use in precursor ion identification. However, this method struggles to identify low-abundant proteins, which are generally of prime biological

interest. Conversely, during a data independent acquisition (DIA) experiment, predefined mass-to-charge ratio (m/z) windows in the MS1 scan are selected for fragmentation and MS2 data acquisition. This produces chimeric MS2 spectra, which potentially contain information for many different peptides which may be co-eluting. Software tools have been developed to analyse and process these chimeric spectra, for the extraction of meaningful biological data. A graphical summary of both acquisition schemes is shown in Supplemental Figure 1.

Sample matrix, or the non-analyte of interest components are an important factor in determining final data quality, as highly abundant contaminants may supress the signal from nearby analytes during data acquisition, resulting in the lack of analyte detection. Multiple proteomic sample preparation methods have been developed over time, prioritizing aspects such as technical ease, preparation time and more importantly protein and peptide purity. A leading method is the Single-Pot Solid-Phase Enhanced Sample Preparation (SP3), which uses modified carboxylate particles to bind to proteins within a detergent-containing lysate[131]. These beads with bound protein are then washed to remove contaminating non-protein components of the sample and detergents before being digested with a proteolytic enzyme, usually trypsin. This method is useful in cases where protein concentration is low, as protein binding to a solid matrix allows for the concentration of protein by removal of supernatant while remaining scalable in terms of initial sample volume and throughput[132,133]. However, the optimization of biological sample collection, protein extraction and digestion, peptide clean-up and data acquisition and processing parameters are all key in establishing a robust, reproducible proteomic workflow to draw meaningful biological conclusions.

2. HYPOTHESIS AND AIMS

2.1. Hypothesis

I hypothesize that HGPS fibroblasts produce harmful EVs that are capable of inducing inflammaging in healthy cells, in turn, resulting in age-associated phenotypic and genotypic changes. Conversely, healthy cells produce regenerative EVs capable of restoring many age-related properties in HGPS cells.

2.2. Objectives

The primary objective of my project is to identify the cargo in age-associated EVs, released by healthy and HGPS cells, that contain mediators of the inflammaging process, with a particular focus on EV-associated proteins.

2.3. Aims

Aim 1: To develop a method to assess EVs contained within conditioned media (CM) from HGPS and healthy fibroblasts.

Aim 2: To identify subsets of EVs with pro/anti-inflammaging proteins.

3. MATERIALS AND METHODS

3.1. Cell Culture- Fibroblasts

Fibroblasts from health and HGPS patients (Table 1) were cultured in Minimum Essential Medium Eagle with Earle's Salts & L-Glutamine (EMEM, 320-005-CL, Wisent Inc.), supplemented with 15% fetal bovine serum (FBS; Wisent Inc.), 50 U/mL Penicillin and 50 mg/mL Streptomycin (Gibco, BRL), at 37°C in 5% CO_2. Cells were seeded at a density of ~7.5×10^5 per T175 flask and passaged every 4- or 5-days, as required. The FBS used was EV-free, produced by a 4-hour ultracentrifugation run of Wisent FBS at 100'000xg to pellet EV and other large particles. The lack of bovine EV marker proteins was confirmed using DDA LC-MS/MS analysis. (Supplemental Table 2).

Table 1: Patient-Derived Fibroblast Cell Lines from Corriell Institute Used in This Study

Cell Number	Status	Age (at sampling)	Sex	Reference
01	HGPS (unknown mutation)	2	Female	AG07493
02	HGPS (LMNA mutant)	8	Female	AG11513
07	Healthy	1	Male	GM05659
08	Healthy	8	Male	GM08398

3.2. Isolation of Extracellular Vesicles from Conditioned Media

Cells from passages 15 were seeded at approximately $1.0x10^6$ or $1.5x10^6$ (HGPS-02) cells per 15cm dish and grown in conditions described above in 3.1. When confluency reached approximately 50%, as much 15% FBS media was removed by pipetting as possible and 30 mL of 5% FBS containing media was added to each dish. Conditioning occurred over 48 hours, resulting in a confluency of 80-100%. Conditioned media (CM) was removed from the cell culture flasks only once and immediately processed for EV isolation or stored at -80°C until processing. The relative or absolute levels of senescent cells before and after conditioning was not assessed.

A method was optimised to concentrate 40 mL of conditioned media down to 250 µL using Amicon Ultra – 15 centrifugal filters with a nominal molecular weight limit of 100 kDa (REF. UFC910024, Merck Millipore). Briefly, filter units pre-equilibrated with phosphate buffered saline (PBS, [Cat. 311-012-LL, Wisent Inc.]) were loaded with 10 mL of concentrated media and spun at 4000 xg for no more than 20 minutes in a centrifuge (Cat. 022625080, Eppendorf) cooled to 4°C with 50 mL tube rotor (Cat. A-4-44, Eppendorf). The process was repeated without removing retentate 3 more times to achieve samples for further processing, the flow-through was sterilised and discarded as waste.

3.3. Size Exclusion Chromatography

Concentrated conditioned media was separated by size exclusion chromatography (SEC) using commercially available columns by Izon following the manufacturers protocol. Briefly, qEVsingle 35 Gen 2 (Prod. ICS-35, Izon Science) SEC columns were equilibrated using 3 column volumes of 0.1µm filtered (Prod. SLVVR33RS, Merck Millipore) PBS. Next, 150 µL of concentrated conditioned medium was loaded onto the resin bed, and a fraction was collected. Subsequent fractions were collected by the addition of 170 µL f of filtered PBS to the resin bed, up to 16 or 20 fractions. Fractions were the aliquoted for proteomic analysis, nanoparticle tracking analysis or for orthogonal assessment of protein contents, then stored at -80°C. Columns were then washed by the addition of 1 column volumes of filtered PBS, 1 column volume of 0.1 M sodium hydroxide in PBS, equilibrated with 1 column volume of filtered PBS and stored in 0.05% sodium azide at 4°C until future use.

3.4. Nanoparticle Tracking Analysis (NTA)

Conditioned medium, concentrated conditioned medium and SEC fractions were assessed for nanoparticle content using a ZetaView Nanoparticle Tracking Analysis system (Particle Metrix, Germany). Samples containing particles were diluted in 0.1 µm-filtered PBS that was degassed using water-bath sonication such that particle count per frame was between 40-200 particles. Data was acquired with the microscope and analysed using manufacturer software using particle bin size = 5 nm, minimum pathlength of 5. Output files were processed with an in-house Perl program with an integrated R module for graphing; notably, the program automatically adjusted particle concentration to account for the dilution factor, which is not provided by default in the ZetaView output files if dilution factors are not set in the software. Result files from this code were also produced for graphing and analysis in GraphPad Prism.

3.5. Protein Extraction and In-Solution Digestion of Proteins and UF-SEC Fractions

Fibroblast cell pellets and SEC fractions were digested using the single-pot solid-phase enhanced sample preparation (SP3) for mass spectrometric analysis. Cell pellets were lysed in 1% sodium-dodecyl sulfate (SDS) in PBS containing 1:500 dilution of protease inhibitor cocktail (Cat. P8340, Millipore Sigma) on ice using a sonicator. Protein concentration of cell lysates was determined using a detergent-compatible Bradford assay. Approximately 20 µg of cell lysate protein was reduced using dithiothreitol (DTT) and alkylated with iodoacetamide (IAA). These lysates were used for SP3 protein extraction using equal amounts of modified carboxylic particles (Cat. 65152105050250 and Cat. 45152105050250, GE Healthcare), for a final mass of 100 µg of beads per sample. Protein binding was induced by the addition of pure ethanol for a final ethanol concentration of 50%. The ethanol and beads were allowed to incubate with protein solutions for 10 minutes, a rotator revolving approximately 60 times per minute. Samples were placed on a

magnetic rack and the beads were left to settle against the side of the tube prior to supernatant being removed. Beads with bound protein were washed thrice with 80% ethanol before being resuspended in 50 mM ammonium bicarbonate (AMBIC) containing 0.25 µg of sequencing grade porcine trypsin (Cat. V511C, Promega). Trypsin aliquots were subjected to a maximum of 3 freeze-thaw cycles. Tryptic digestion of bound protein occurred overnight, for at least 18 hours, at 37°C. Digests were removed from the beads and frozen at -80°C until use.

Protein isolation and digestion occurred similarly for SEC fractions, with the following notable modifications. Liquid fractions were spiked with a concentrated solution of SDS containing protease inhibitors such that the final concentration of SDS was 1% and protease inhibitor was 1:500. Protein concentration was unable to be determined using conventional methods, thus, the entire sample aliquoted for proteomics was digested at once. Protein reduction and alkylation occurred as above, with reduction time being increased to expose the samples to heat for a longer period to aid in EV breakdown. Modified carboxylate particles were added such that the final concentration of beads during the ethanol binding step was at minimum 0.5 µg/µL, as suggested by the authors of the SP3 method when dealing with large-volume and low-concentration samples[131]. All other steps were carried out as described above.

3.6. Mass Spectrometry

Frozen peptide digests were thawed then acidified for a final concentration of 0.1% formic acid, to give peptide a net positive charge. Acidified cell lysate digests were transferred into clear glass autosampler vials with silicone septa. Due to the large quantity of SEC fractions that were processed, acidified SEC digests were loaded into 96-well “V-bottom” plates then sealed with foil sealers using gentle heat for analysis by mass spectrometry. Plates were siliconized to avoid sample loss by adsorption using 10% (v/v) SurfaSil siliconizing fluid (Cat. TS-42801, ThermoScientific)

prepared in toluene and baked at 75°C for one hour, then rinsed with ddH_2O [134]. As the foil sealer is not self-closing, digests withdrawn from plates were only sampled once to prevent increases in peptide concentration due to solvent evaporation. Vials of 25 mM AMBIC wash blank solution were also prepared in autosampler vials with pre-slit septa, and replaced as needed, about every month. These were stored at 4°C until loaded into the chilled autosampler.

Mass spectrometric analysis was performed using an UltiMate 3000 RSLCnano liquid chromatography system interfaced with an Orbitrap Eclipse Tribrid mass spectrometer. Analysis involved injection ~0.8 µg of the peptide sample onto a 300 µm I.D. × 0.5 mm 3 µm PepMaps® C18 trap (ThermoScientific) followed by separation on a 100 µm I.D. × 10 cm 1.7 µm BEH130C18 nanoLC column (Waters, Milford, MA, USA) using a 72 min step-wise gradient from 6% to 85% solvent B (100% acetonitrile and 0.1% formic acid). The eluted peptides were ionized by electrospray ionization for either DDA analysis and the data for MS/MS was acquired in the Orbitrap of the instrument on ions with mass-to-charge values between 375 and 1800 at a resolution of 60,000 followed by higher-energy collisional dissociation fragmentation and MS2 scans to acquire further data about peptide identity. All parameters were identical for DIA analysis, each MS1 scan was analyzed using 53 windows of 10 m/z in width with 1 m/z overlap covering the range from 145 – 1450 m/z using a resolution of 15,000 for MS2 scans. Maximum injection time was set to 40 ms with normalized AGC target of 200 %, resulting in a maximum cycle time of 2120 ms. To reduce batch-effects at the mass spectrometric level, all samples to be compared were run during the same batch, with quality control samples run before and after the samples for analysis and biological interpretation.

3.7. Processing of Mass Spectrometry Data

3.7.1. Data Dependent Acquisition (DDA) Experiments

RAW files produced by Xcalibur were processed in FragPipe (v22.0), using the 'LFQ-MBR' (Label-Free Quantitation Match Between Runs) workflow[135]. Briefly, files were processed using peak matching precursor and fragment mass tolerance of ±20 ppm, strict tryptic digestion and a maximum of 1 missed cleavage per peptide. Peptide length was 7-35 amino acids, with a mass range of 500-5000 Da. Fixed modifications included alkylated cysteine (+57.02146 Da) and variable modifications included oxidation of methionine (+15.9949 Da) and acetylation of peptide N-termini (+42.0106 Da).

3.7.2. Data Independent Acquisition (DIA) Experiments

Due to the experimental design of our DIA method, output RAW files are generally incompatible for direct processing with many proteomics analysis tools, as the MS isolation windows are staggered with a small m/z overlap with the adjacent window. Using MSConvert version 3.0.23227-d5af1be)[136], RAW files were demultiplexed and outputted as mzML files using the following parameters: peakPicking vendor msLevel=1- , zeroSamples removeExtra 1- . Identification and quantification occurred using DIA-NN with spectral library, via the FragPipe graphical user interface[137]. All settings were turned off, except for "Quantify with DIA-NN" under the Quant DIA tab, FDR was set at 0.01%, with "Robust LC (high precision)".

3.7.3. Offline Generation of Spectral Libraries for DIA Data Processing

Spectral libraries were generated using MSFragger DIA through the FragPipe interface[137]. RAW DDA files and DIA mzML files were processed using peak matching precursor and fragment mass tolerance of ±20 ppm, strict tryptic digestion and a maximum of 1 missed cleavage per peptide. Peptide length was 7-35 amino acids, with a mass range of 500-5000 Da. Fixed modifications included alkylated cysteine (+57.02146 Da) and variable modifications included

oxidation of methionine (+15.9949 Da) and acetylation of peptide N-termini (+42.0106 Da). The final library contained 5306 proteins.

3.8. Post Processing and Statistical Analysis of Peptide Lists

DIA-NN peptide output files (report.pr_matrix.tsv) were filtered using Microsoft Excel (Version 2411) to include only peptides that were not common or custom contaminants within the spectral library, were uniquely mapped to a single protein, and were quantified at least three times in independent samples. This filtered list comprising of protein name, peptide sequence, number of times quantified and MS/MS intensity values per sample was exported to a tab-separated file for further processing.

For the processing of whole-cell lysate (WCL) data, a custom-developed R script was used to normalize peptide intensities using median normalization and to impute missing intensity values using the Perseus method[138]. Perseus-style imputation replaces missingness by a value pulled from a normal distribution with a downshift of 1.8 standard deviations from the median of observed values with a width of 0.3 in the log2 space. Various quality control plots were also produced to assess data integrity and monitor modifications to intensity distributions throughout the data processing pipeline. Peptide-level data was then aggregated to a protein-level summary by the summation of the top three most intense peptides per protein as is common in mass spectrometry-based proteomics.

Analysis of pooled and individual UF-SEC fractions was performed using the FragPipe-Analyst tool with the DIA-NN protein group output files (report.pg_matrix.tsv)[139]. Analysis parameters used were as follows: Data Type, DIA; Normalisation type = no normalization; Imputation type = Perseus-type; Type of FDR correction = Local and Tail area-based.

Differential protein expression analysis for WCL occurred using volcano plots generated in R, where fold change and p-values corrected using the Benjamini-Hochberg method were computed. Differential expressions were deemed significant if fold change was equal to or greater than 2, with an associated corrected p-value of less than or equal to 0.05. Details about specific R packages and their implementations are available as Supplemental Table 1. UF-SEC volcano plots were generated using the output of FragPipe-Analyst.

3.9. Manual Validation of Mass Spectrometric Data

Proteins of interest were manually validated using the Skyline software from The MacCoss Lab[140]. Peptides identified using FragPipe were added to the targets tab, or FASTA formatted protein sequences were imported into the software for in-silico tryptic digestion, then RAW (DDA) or mzML (DIA) files were imported[137]. Manual validation occurred at the MS2 level (fragment ion / peptide fragment), which was then mapped to an MS1 peak (parent ion / peptide). At least one sample from the set of files analyzed was required to have an MS2 fragmentation pattern of at least three strong fragments for peak identification, and subsequently the signal needed to map to an MS1 peak for quantification. When MS2 signals were not observed in a file, the appropriate peak was identified using the MS1 spectrum, and nearby MS1 "reference peaks". To assist in the manual selection of peaks, Skyline ion match tolerance was set at 0.5 m/z, which functions to highlight product ions in the experimentally collected spectra to what was theoretically calculated for interpretation by the human rater.

3.10. Statistical Analysis of Manually Validated Proteomics and *in vitro* Data

Statistical analysis was performed using GraphPad Prism Software (GraphPad Software Inc). Data are presented as mean ± SD. Data was compared using the Student's t-test following the

assessment of normality by the Shapiro-Wilk test. Comparisons between multiple groups were performed using a one-way ANOVA (analysis of variance) test followed by Tukey's post-hoc correction, after normality was assessed following the Shapiro-Wilk test. The threshold for statistical significance was set at p-value ≤ 0.01, and P values are reported wherever appropriate. This paragraph describes the statistical analyses used unless explicitly or otherwise noted in the figure and / or table caption.

3.11. Bioinformatics and Network-Based Analysis

Gene ontology enrichment analysis searches were performed using the STRING application[141] within Cytoscape[142] against all databases. Redundant term removal was set at 0.5, while only terms with p-values ≤ 0.001 were deemed significant for graphing in GraphPad Prism. Using Cytoscape and STRING, physical protein-protein interaction (PPI) maps were generated for the EV protein, with the PPI confidence threshold set at 0.95.

4. RESULTS

4.1. Optimization of HGPS EV isolation and proteomics methods.

4.1.1. Optimizing conditioned media processing for proteomics analysis of EV isolates.

The study of EVs, from biofluids, conditioned cell culture media, or other sources requires a method to isolate the particles for various physical and molecular characterization experiments[107]. In the context of this project, it was determined that the fibroblast cells derived from HGPS patients were incompatible with true FBS starvation down to 0% (data not shown). The result of such starvation lead to cell death before the required 48 hours of media conditioning for EV collection, no assessment was performed to determined the method of cell death which was observed. This was, somewhat expected as serum depletion is sometimes used as a method to synchronize cell cycle for certain cell biology applications[143]. However, others have reported success in serum starvation of similar HGPS cell lines for up to 48 hours[144]. As the HGPS fibroblasts in cell culture may likely form at least two distinct populations, either replicative or senescent; removal of serum may have been a sufficiently stressful stimuli to induce irreversible changes in the culture that may culminate in apoptosis[145]. Indeed, results presented by others, such as SA-β-Gal staining, may support the two-population hypothesis[146,147]. Furthermore, the increased cell death observed in these cultures would increase the burden of contaminating apoptotic bodies and other forms of cellular debris in the final EV isolate. It was determined that serum reduction down to 5% FBS (from supplementation at 15% under normal culture conditions) was the minimum serum requirement without significant modification in cellular, and presumably, EV phenotype. The latter was not tested by our laboratory but reported by others[148–150].

The reduction in serum served a twofold purpose, first to reduce the amount of contaminating protein aggregates which may be of serum origin, or artefactually produced by

sample handling which complicates NTA data acquisition and to reduce the protein contamination for mass spectrometric analysis. The first challenge could have been addressed by detergent-based differential solubilization methods, which would leave EVs intact and solubilise protein, but is not an accepted method to purify EVs from any biological sample, despite being a useful method for optimising EV size measurement[151,152]. Secondly, the reduction of FBS in CM was required due to the high abundance of contaminating protein of bovine origin, like albumin (ALB), which hinders effective protein identification and quantification by MS[153]. It is generally accepted that the concentration of protein in heat-inactivated FBS is approximately 3 mg/mL, however, this estimate was found to be conservative as the experimentally determined protein concentration in this project was found to be near 6 mg/mL (data not shown). Therefore, CM containing 15% FBS may have up to 0.9 mg/mL of contaminating protein, producing a complex sample matrix.

A final source of contamination that was relevant was bovine-derived EVs[154]. This was mitigated using in-house prepared EV-free FBS, which is cost-effective when compared to commercial alternatives and simple to produce by ultracentrifugation of FBS at 100,000 xg for 4 hours, as suggested by MISEV and consistent with protocols reported by others[106,107,148]. The lack of bovine-specific sequences for EV markers, notably CD63, CD9, PDCD6IP (ALIX), TSG101 and CD81 was confirmed by data dependent mass spectrometric analysis of concentrated FBS, produced in a way that mimics the optimal method of EV isolation described in detail below (Figure 3A) [109]. As expected, ALB dominated the protein list, followed by gelsolin (GSN); proteins from the complement system and serine protease inhibitors (SERPIN*) were also identified and consistent with what is known about FBS. Human EV protein markers (Figure 3B) were absent and validated using parallel reaction

monitoring mass spectrometry (PRM-MS, data not shown). Additional data on the FBS proteome are presented in Supplemental Table 2.

A

Protein Name	Proportion of LFQ Intensity	Protein Name	Proportion of LFQ Intensity
ALB	32.29%	AGT	0.52%
AHSG	10.81%	FAM186A	0.45%
GSN	7.78%	SERPINA3-3	0.42%
TF	5.69%	CLEC3B	0.38%
GC	4.19%	HBB	0.35%
AFP	3.31%	INHCA	0.35%
C3	2.22%	LTF	0.34%
SERPINF1	2.04%	SERPINA3-8	0.31%
SLC47A1	1.77%	C4	0.31%
SERPINA6	1.61%	APOE	0.30%
A1BG	1.58%	IPLA	0.29%
APOA1	1.54%	CFH	0.29%
A2M	1.26%	ORM1	0.26%
PF4	1.25%	ADIPOQ	0.24%
SERPINA1	1.24%	FGA	0.24%
SERPINA5	1.02%	APOA4	0.24%
KNG1	0.99%	FN1	0.23%
SERPINC1	0.94%	F2	0.22%
FETUB	0.83%	AFM	0.22%
HBA	0.83%	APOA2	0.21%
C9	0.80%	AMBP	0.21%
ITIH4	0.75%	SERPINA7	0.21%
ITIH2	0.67%	IGFBP2	0.20%
KNG2	0.66%	ACTB	0.19%
SERPINA3-1	0.62%	SERPINA3-7	0.18%
PLG	0.60%	HPX	0.16%
APOH	0.57%	C7	0.14%
VNN1	0.57%	CLU	0.14%
RPOC1	0.55%	SERPINA3-5	0.14%
ITIH3	0.53%	ACT3	0.14%
CFB	0.52%	SERPINA3-6	0.13%
SERPINF2	0.52%		

B

EV Marker Proteins	
CD63	HSP90AA1
CD9	HSPA8
PDCD6IP	ANXA5
TSG101	ENO1
CD81	PKM
GAPDH	HSP90AB1
FLOT1	YWHAZ
ACTB	PGK1
ANXA2	FLOT2
SDCBP	YWHAE

C

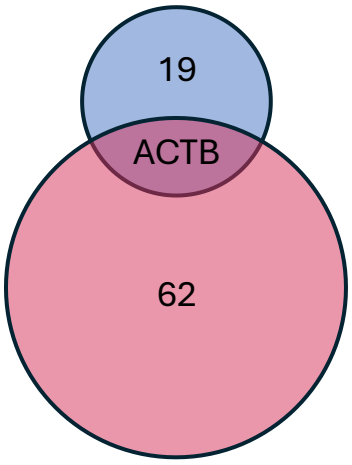

Figure 3: Proteomics of extracellular vesicle-free fetal bovine serum.

(A) List of proteins identified in EV-free FBS sorted in descending order of "Proportion of LFQ Intensity". Proteins that contributed less that 0.1% of the total LFQ intensity are not included in this table. **(B)** The top 20 most reported EV markers per Vesiclepedia[109]. **(C)** Venn diagram demonstrating the overlap of the FBS proteome (red) and the top 20 of the most reported EV markers per Vesiclepedia (blue). The only common protein between both datasets was ACTB.

4.1.2. An optimized EV isolation method for deeper proteome coverage.

Next, I was interested in determining an optimal EV isolation method for HGPS cellular and EV proteome. For this project, we defined an optimal method as one that produces a high number of protein identifications using the commonly available academic license software FragPipe, with a filtering threshold of 5% false-discovery rate[137]. However, to improve my ability to provide biological interpretation of the data, I also sought to identify a method which would have a large number of high-confidence protein quantifications using software and manual validation techniques, such as Skyline[140]. I tested three methods of EV isolation from CM that are compatible with mass spectrometry, namely ultracentrifugation (UC)[155], size exclusion chromatography (SEC) and ultrafiltration size exclusion chromatography (UF-SEC). These methods are commonly reported in studies requiring EV isolation, and internal, unpublished data[i] from our lab suggests that these produce the highest purity EV isolates for mass spectrometric analysis[107]. Furthermore, these UF and SEC-based methods are MS compatible, in contrast to polyethylene glycol (PEG) and other polymer precipitation workflows which are deployed in kit formats and require additional cleanup steps due to poor removal of contaminating proteins, which may result in the increased loss of sample. I did not assess density gradient ultracentrifugation methods in this project, however, this method is a commonly used alternative[156].

To ensure the most comparable data as possible, the experimental design consisted of dividing a single large volume of media into three aliquots, while using identical input volumes for each SEC method (Figure 4A). DDA was used for this initial assessment, as I expected it to produce a more conservative number of protein identifications when compared DIA.

[i] Data acquired by Alexandra Star with Arsalan Haqqani and Jagdeep Sandhu. Size exclusion chromatography (SEC) outperforms many kit-based EV isolation methods. Manuscript in preparation by Star *et al.*

Preliminary assessment of the CM with and without ultrafiltration led to an approximate 100-fold increase in protein concentration (Figure 4B), and 1000-fold increase in particle count (Figure 4C), suggesting a relative enrichment of particles of about 10-fold. The expected concentration factor would be 160-fold, as 40 mL of conditioned media was concentrated down to 250 μL. There was little difference in the size distribution of the particles before and after ultrafiltration, suggesting this manipulation doesn't bias towards a specific subpopulation of particles (Figure 4C). MS analysis of the 16 SEC fractions of conditioned media without prior concentration led to a total of 133 protein IDs, of which 15 were EV markers as indexed on Vesiclepedia; no tetraspanins were observed (Figure 4D and E). However, when concentrated media was subjected to SEC (the UF-SEC method), 730 proteins were identified which is equivalent to an increase of over 300%, of which 95 were listed in the top 100 Vesiclepedia EV markers, including tetraspanins CD9, CD63 and CD9. Intermediate to these two extremes was UC, which led to the identification of 85 EV markers, lacking YWHAZ (14-3-3ζ) and chaperonins. An increase in non-EV proteins was also observed with respect to the UC method. With this data, I concluded that UF-SEC would be the optimal method to pursue for detailed analysis of the insoluble HGPS secretome, as it offered relative enrichment of particles with respect to protein, and an increase in EV marker identification.

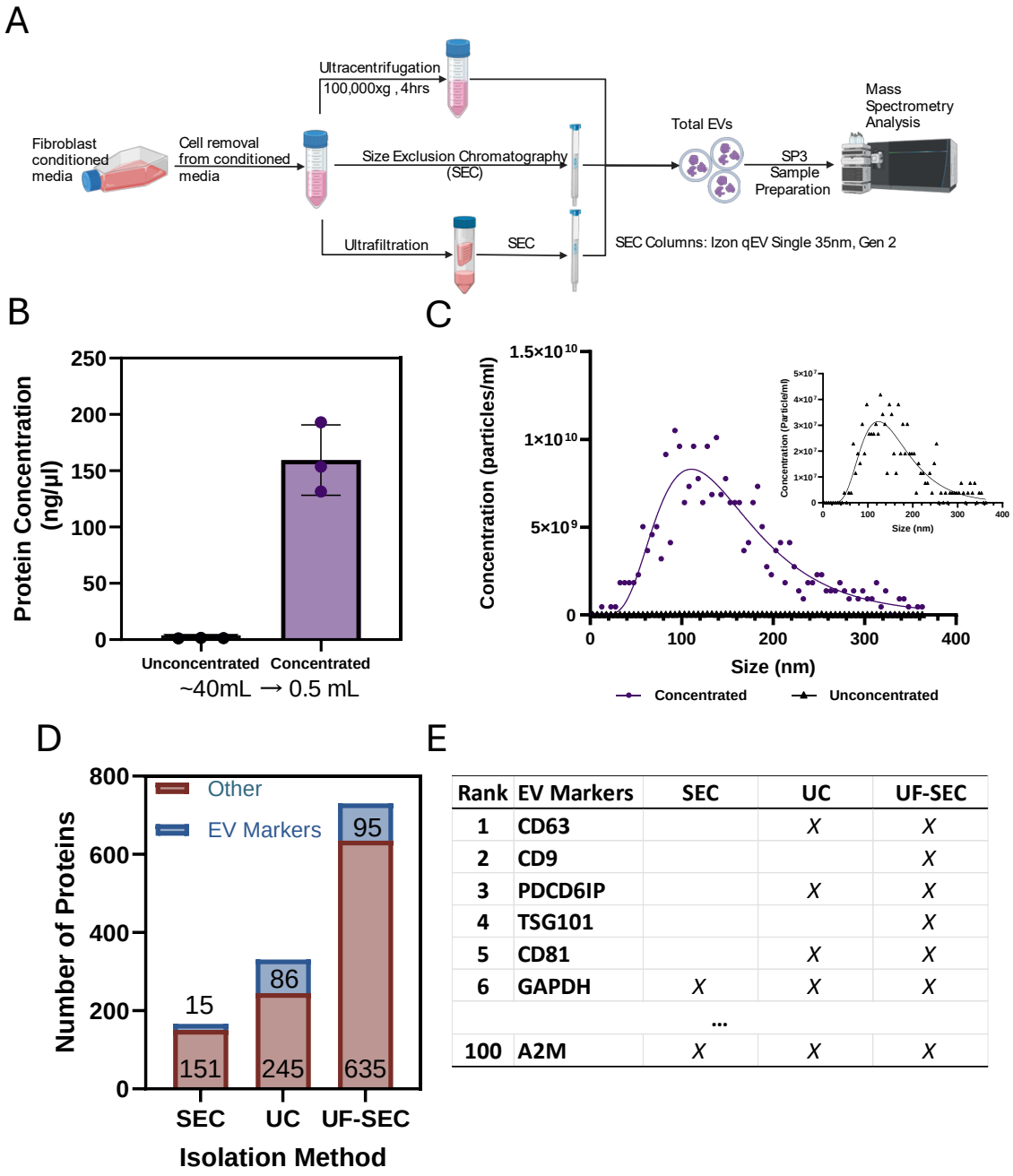

Rank	EV Markers	SEC	UC	UF-SEC
1	CD63		X	X
2	CD9			X
3	PDCD6IP		X	X
4	TSG101			X
5	CD81		X	X
6	GAPDH	X	X	X
		...		
100	A2M	X	X	X

Figure 4: Comparing EV isolation methods.

(A) Workflow of EV isolation methods. **(B)** Comparison of the protein concentration by Bradford assay and **(C)** nanoparticle concentration by nanoparticle tracking analysis in concentrated and unconcentrated conditioned fibroblast media. Points are experimental data while the line is a log-normal fit to the experimental data. **(D)** Plot quantifying the number of protein (red) and EV markers (purple) using each method. **(E)** Representative list of top EV markers identified by each method. Data was acquired as n=1 biological replicate. MSFragger was run at 20 ppm mass tolerance for database searching. SEC and UF-SEC contain pooled data from 16 mass spectrometric runs representing fractions 1-16.

4.1.3. Characterization of the SEC fractogram to identify fractions enriched with EVs.

As the UF-SEC method was identified as the most optimal approach of detecting EV proteins in the CM, I sought to better understand the composition of each fraction and target specific subsets for further detailed analysis. Using the Izon qEV Single 35nm Gen2 commercially available SEC columns, I was able to recover approximately 80% of the input protein when collecting 25 fractions and quantifying protein using the standard Bradford method. Protein loss is likely due to binding to the column resin; phenol red elution in fractions beyond 16 may also interfere with protein quantification using this technique. However, as the EV-containing fractions contain a very low amount of protein, and given the small size of phenol red, utilization of phenol red-free media strictly for this assessment was not warranted.

An increase in particle concentration and decrease in particle size was observed starting in fraction 6 (Figure 5A and C), which is approximately where sample loaded onto the resin bed begins to elute due to column volume. This is expected as larger particles should elute first, whereas smaller particles are retained in the resin for longer. Along with this, EV-specific markers begin to elute in the sixth fraction (Figure 5B). When considering the recommendations suggested by the MISEV 2023 statement, our samples were unsurprisingly contaminated with blood-derived bovine proteins associated with the EV corona (i.e., complement factors), adhesion molecules recovered with EVs, and potentially exomere or supermere species[107]. Specific attempts at recovering adequate numbers of exomeres and supermeres from the UF-SEC fractions for proteomic analysis were futile, successful isolation of these particles in this disease could have been an interesting addition to the field. However, no specific attempts were made to establish standard protocols for the isolation of these NVEPs[157,158]. Notably due to the small sample size, the non-vesicular nature of these particles, the lack of specific functions associated to them, and their limited relevance in extracellular particle research, they were deemed out of scope for this

project[157,158]. Inclusion of these NVEPs in future studies may be meritorious to gain deeper insight into these particles as the field is still nascent. Further discussion about the isolation of NVEPs is included later (Section 5.1). A non-exhaustive list of selected markers in each protein content-based EV characterization categories from MISEV 2023 is presented as Supplemental Figure 2, which shows presence of both surface and cargo EV proteins in fractions 6-10.

In fraction 10 and beyond, protein content increased due to the elution of soluble proteins from the SEC column, mainly from contaminating bovine proteins, such as bovine serum albumin (BSA, Figure 5B). Attempts at differential solubilization of proteins while keeping membrane-bound vesicles intact, as suggested by Osteikoetxea and colleagues, were unsuccessful, and fractions beyond 14 were not assessed by NTA[152]. From this data, I considered fractions 6-10 as the purified collection volume (PCV) for EVs, to be assessed in greater detail for biological interpretation in subsequent experiments.

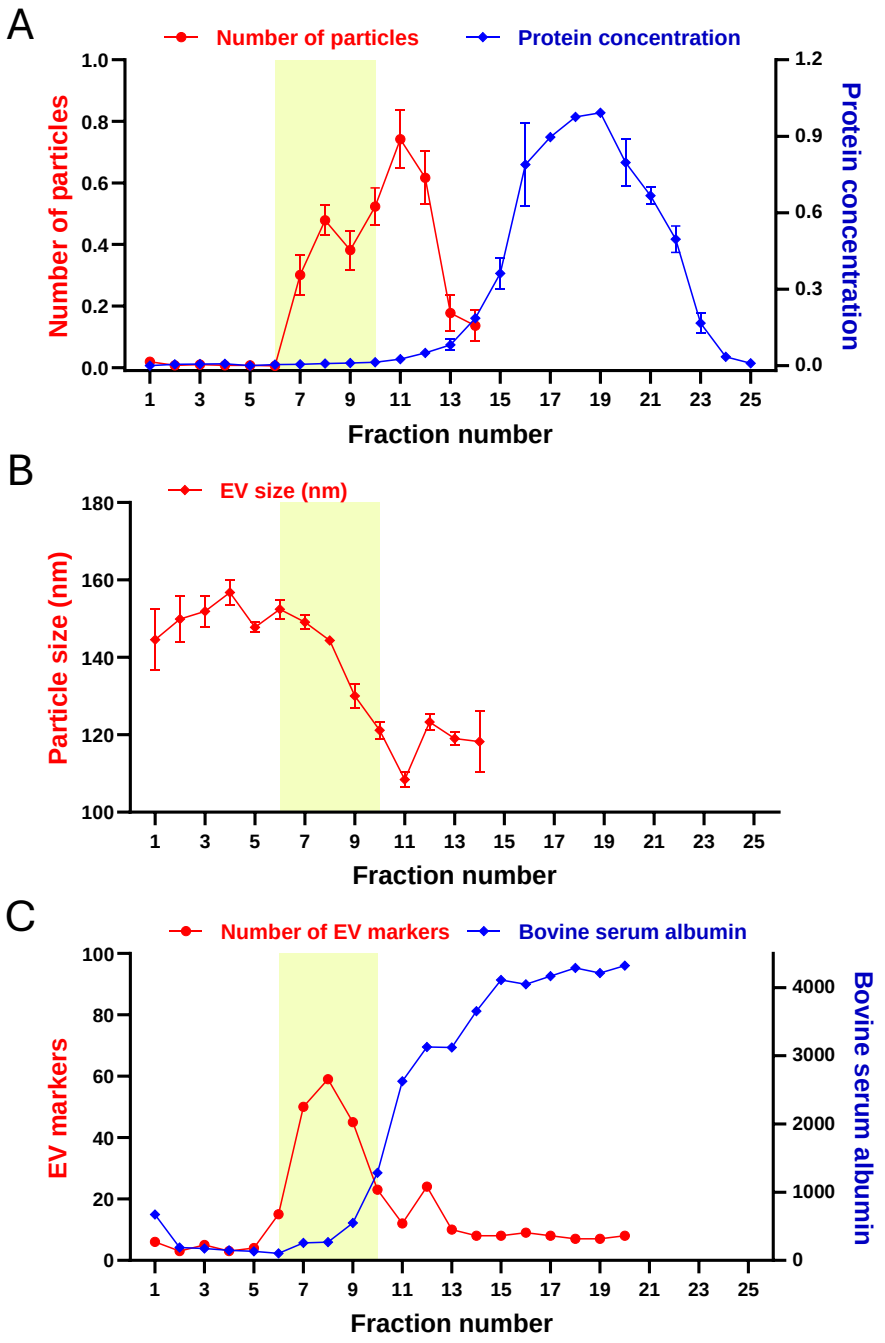

Figure 5: Identifying EV-enriched SEC fractions.

(A) Fractogram of protein concentration (n=2, maximum = 12.2 mg/mL) and particle count from NTA expressed as a percent of maximum. (n=6, maximum= $112.5*10^{10}$ particles/mL). **(B)** Mean particle size in each fraction as determined by NTA. Data is presented as mean ± SD, if bars are not shown, they are smaller than the point size or n=1. The yellow area represents the purified collection volume, which contains EVs. Fractions beyond 14 were not analyzed by NTA due to the increase in protein contamination. **(C)** Count of EV markers as indexed on Vesiclepedia (n=1, maximum=59 markers) and number of spectral counts of contaminating bovine serum albumin peptides (n=1, maximum= 4322 spectral counts). The instrument's detector was likely saturated with BSA peptides in fractions beyond 15.

4.2. An optimized mass spectrometric method for low-protein samples

The next experimental parameter to optimize was data acquisition by mass spectrometry. I tested two distinct data acquisition schemes, data dependent acquisition (DDA) and data independent acquisition (DIA). A graphical representation of each scheme is demonstrated in Supplemental Figure 1.

4.2.1. Comparing acquisition methods in whole cell lysate

I first started with whole cell lysates (WCL), to test the two methods in samples where I could confidently quantify protein and mass loaded onto the liquid chromatography column that was interfaced with the mass spectrometer.

DDA demonstrates (Figure 6A and C) good MS2 fragmentation patterns, like that of parallel reaction monitoring (PRM), which has emerged as a gold-standard for targeted quantitative proteomics[159]. However, when comparing the number of points across the MS2 chromatographic peak, DIA outperformed DDA (Figure 6B and D). Despite observing a good fragmentation pattern at MS2 with DDA, the peak areas of the precursor ions at MS1 for low abundant peptides were poor and not quantitatively reliable. PRM showed superior results compared to both methods (Figure 6). However, PRM is not suitable for large scale discovery proteomics, as it is much lower throughput than DDA and DIA, making it more suitable for targeted validation.

When performing large scale proteomic experiments and exploratory data analysis, automated software packages are used to pick peaks and quantify peptides and protein from mass spectrometric data files[160]. This becomes increasingly challenging when considering the presence of missing values, which may be the result of a biological difference or instrumental limitations[161]. When comparing DDA and DIA methods using HGPS and healthy controls (HC) cells lysates, the missingness was notably higher in DDA (Figure 6E). This difference suggests that in WCL, DIA

provides more consistent coverage, making it the superior untargeted proteomic method in these experimental conditions. The higher missingness in DDA may affect data reliability and completeness, highlighting the advantages of DIA for proteomic analyses.

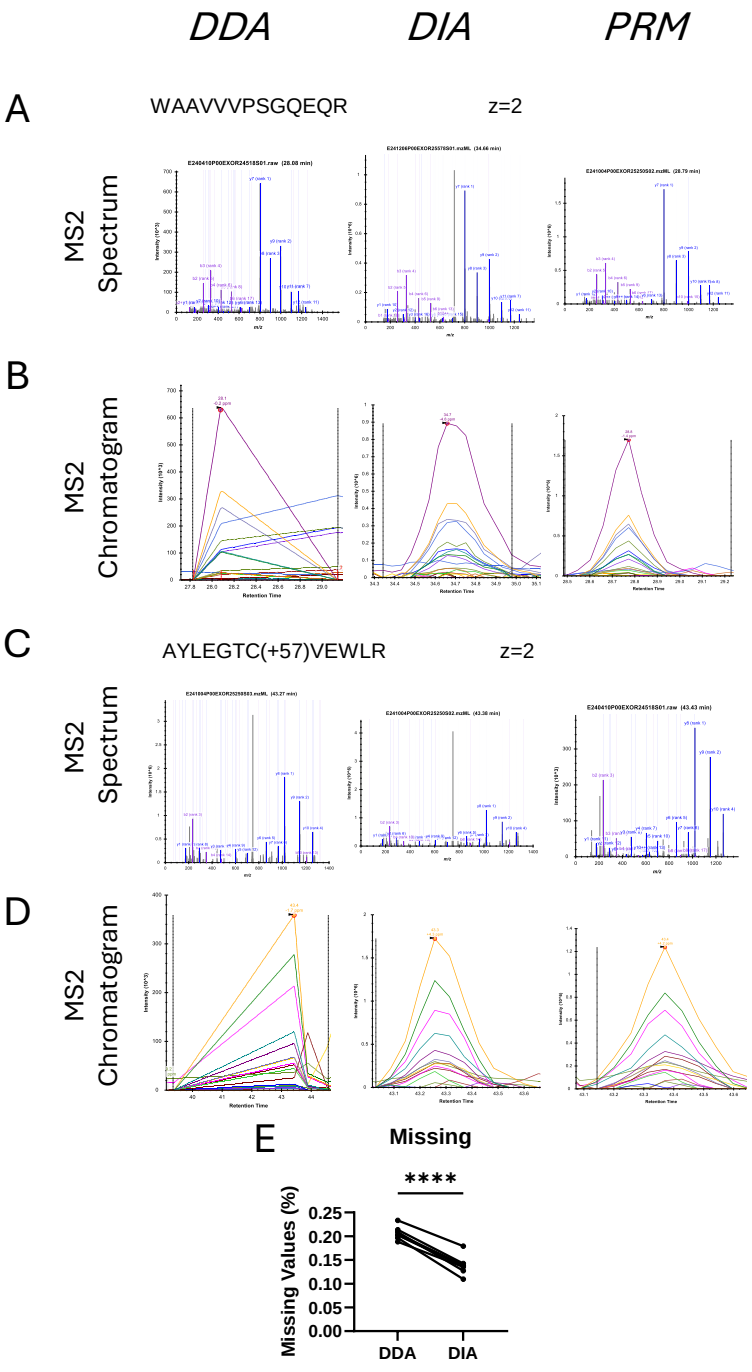

Figure 6: Comparing the quality of mass spectrometry results among different acquisition methods.

(A) Representative MS/MS spectra from tryptic peptide WAAVVVPSGQEQR and the **(B)** MS/MS chromatogram of the same peptide. **(C)** Representative MS/MS spectra from the tryptic peptide AYLEGT[C]VEWLR with carbamidomethylation (alkylation) of cysteine residue. **(D)** MS/MS chromatogram. MS/MS spectra are from the chromatographic peak apex (black arrow). **(E)** Proportion of missing values produced by FragPipe quantification (n=8). A paired t-test was used to compute the p-values. Digests from WCL were used for these analyses. **** p-value < 0.0001.

4.2.2. Comparing acquisition methods in UF-SEC fractions

Given the differences in the sample matrix between WCL and UF-SEC fractions, along with a notable difference in the quantity of peptide loaded onto the LC column during LC-MS/MS analysis, it was valuable to assess both DDA and DIA in the context of UF-SEC before deciding on the optimal method. From the data presented in Figure 4, and similar data not shown, I hypothesized that DIA would remain superior to DDA in terms of protein identifications in samples with low protein abundance. To test this hypothesis, I analyzed fractions 6-10, corresponding to the PCV established in Figure 3, by DDA and DIA. To ensure a fair comparison, files from the same method were analysed together in FragPipe against the same custom human UniProt proteome with FBS contaminating protein sequences spiked in[129,160]. Match-between-runs (MBR) was allowed to maximize protein IDs[162]. DIA without an *a priori* generated spectral library, where the DIA files were used to both generate the library and subsequent quantification proved to identify less protein with respect to DDA (Figure 7A). Missing values remained largely similar for both methods (Figure 7B). However, when building a library with WCL data and the DIA to be used for quantification, greater number of proteins were identified in the PCV with respect to DDA (Figure 7A) with little change in missingness (Figure 7B). Using DIA, raw protein intensities were approximately one order of magnitude lower when compared to DDA (Figure 7C), because DIA (and PRM) intensities are from fragment ions (MS2) while DDA intensities are from precursor ions (MS1). From this data, I concluded that DIA, when using a spectral library containing all data collected during this project, would be the most suitable acquisition method for proteomic analysis of samples containing low amounts of protein.

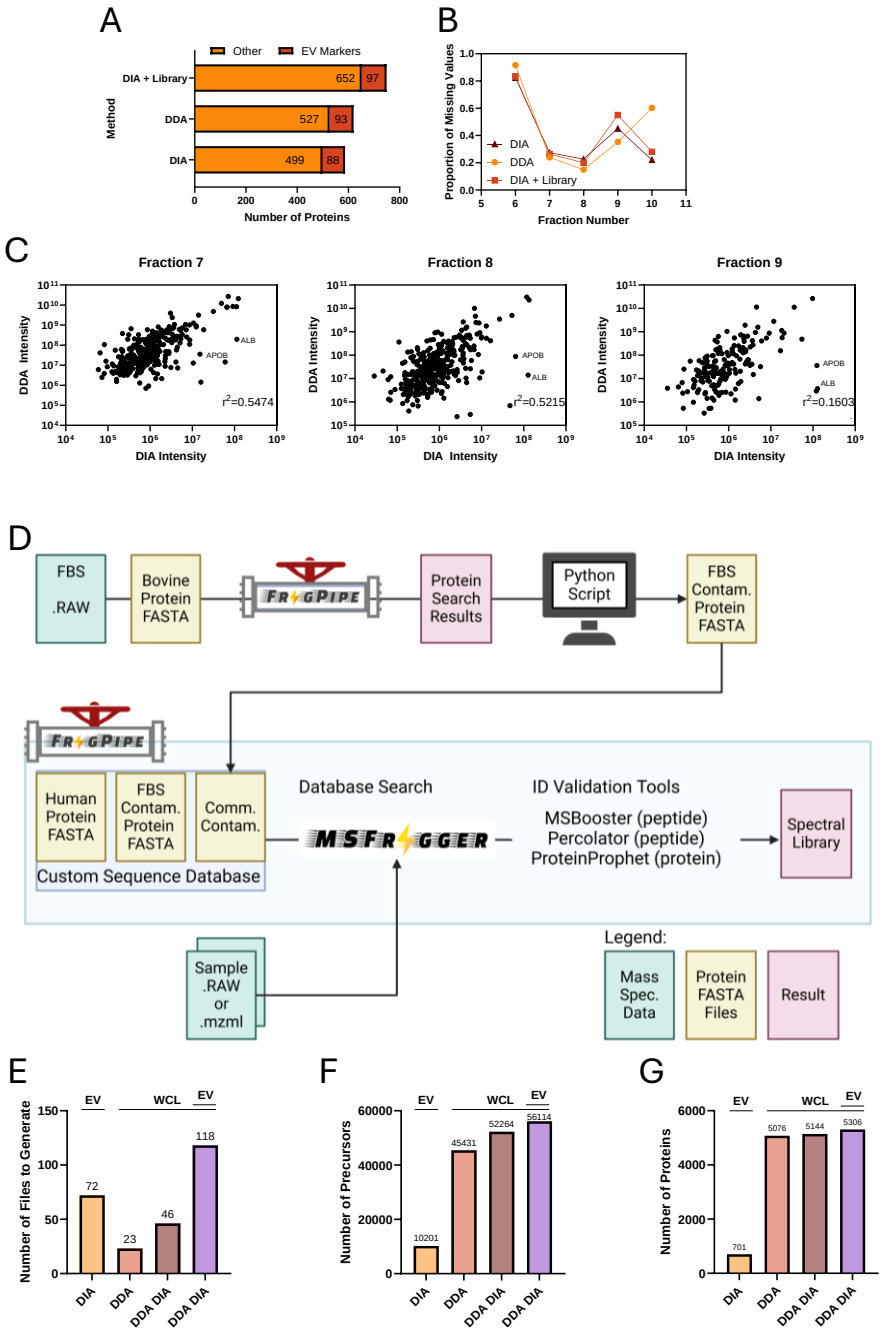

Figure 7: Comparing DDA and DIA in UF-SEC Digests.

(A) Number of proteins and EV markers quantified using DDA and DIA. **(B)** Proportion of missing values in each UF-SEC fraction for each method. **(C)** Correlation between raw intensities of DIA and DDA for fractions 7, 8 and 9. **(D)** Schematic workflow for processing mass spectrometer output files (green) and FASTA protein sequence files (yellow) into spectral libraries. In the first step, a background of contaminating FBS protein is identified. In the second step, FragPipe is used to download the human proteome FASTA file, with our custom FBS contaminants "spiked-in" along with the common contaminants (ex: porcine trypsin) and tools within FragPipe are used to generate the final spectral library for DIA data processing. **(F)** Number of files used for generation of each of the spectral libraries. **(F)** Number of precursor ions and proteins **(G)** represented in each library Abbreviations: Comm. Contam. Common contaminants; Spec. Spectrometry.

4.2.3. Building spectral libraries for DIA data processing from experimental data of diverse sample types

As proteomic analysis of UF-SEC fractions using DIA data acquisition and a spectral library built from previous results was determined to be the most effective method of identifying protein in the sample, I sought to investigate the effects of using different result files (from WCL and UF-SEC fractions) on the final library. The goal was to identify if including result files from different sample types yielded a measurable and significant difference in the library. The workflow for library generation is presented in Figure 7D. Briefly, using knowledge of the FBS proteome (Supplemental Table 2), I was able to produce a customized, project-specific set of contaminants to append to the "common contaminant" list provided by Fragpipe (i.e., porcine trypsin). Then this list of contaminants, along with human protein sequences and decoys (reverse protein sequences) for FDR calculation, was used as a custom sequence database (41214 entries, 50.0% decoy) for spectral library generation.

Using only UF-SEC DIA files lead to a library containing approximately 10,000 precursors covering 701 proteins (Figure 7F and G). Adding WCL data allowed for a large increase in identifiable proteins, which are cell-lysate specific proteins. When combining WCL data with EV data, the library size increased by 162 proteins, most of which were enriched in EVs. Therefore, including both data from WCL and EVs in the spectral library will allow for the identification of positive EV markers such as tetraspanins, and negative EV markers like GM130 a protein of the Golgi apparatus. In this project, the added time cost of the extra mass spectrometric runs was negligible, as no runs were explicitly for the purpose of library generation, as is common with other spectral library generation methods such as using peptide pre-fractionation for samples designated for library generation and no biological interpretation. Given these results, I selected the largest library, as I wanted the ability to quantify the greatest number of proteins as possible.

This decision also allows the inclusion of cellular protein in the library, permitting some determination of EV preparation purity.

4.3. Application of optimal methods to analyze proteomes of HGPS fibroblasts and EVs

With Aim 1, and method development work completed, analysis of biological data was of prime importance to complete Aim 2. An understanding of cellular protein expression can help guide further inquiry into EV proteomic studies. Therefore, I decided to first investigate the protein expression in the fibroblasts used to produce these EVs. This, study includes two HGPS patient-derived immortal cell lines and two from healthy, aged-matched controls (Methods, Table 1).

4.3.1. The proteome of HGPS fibroblast WCL

My first goal was to establish a global understanding of protein expression. This analysis was completed while keeping both HGPS patient data separate, as HGPS-01 has an atypical HGPS genotype with uncharacterized mutation, whereas HGPS-02 has the classical LMNA nucleotide C2036T substitution in the region coding for exon 11, leading to the activation of a cryptic mRNA splice site and a 50 amino acid deletion at the protein level[74]. Each patient had a similar number of dysregulated proteins, with a comparable number of up- and down-regulated proteins (Figure 8A and B). To further investigate these differences, a heatmap was generated using the normalized and imputed protein intensity data for the significant proteins identified in the volcano plots. As shown in Figure 8C, there were two large categories of up- and downregulated proteins. The upregulated proteins were more evident in the classical HGPS fibroblast cell line. The dysregulation we have identified is consistent with previous results presented by others, such as in WNT5A[163]. Some other dysregulations were novel or unable to be identified in the progeria literature. This analysis also revealed, despite some dysregulation

observed in our data was not significant in both HGPS patients, the change in most of these proteins were similar in both cases. Enrichment analysis, with redundant terms removed, showed that proteins with increased expression in HGPS were associated with organelles and endomembrane systems, while proteins with decreased expression were linked to the extracellular space and matrix (Figure 8D and E).

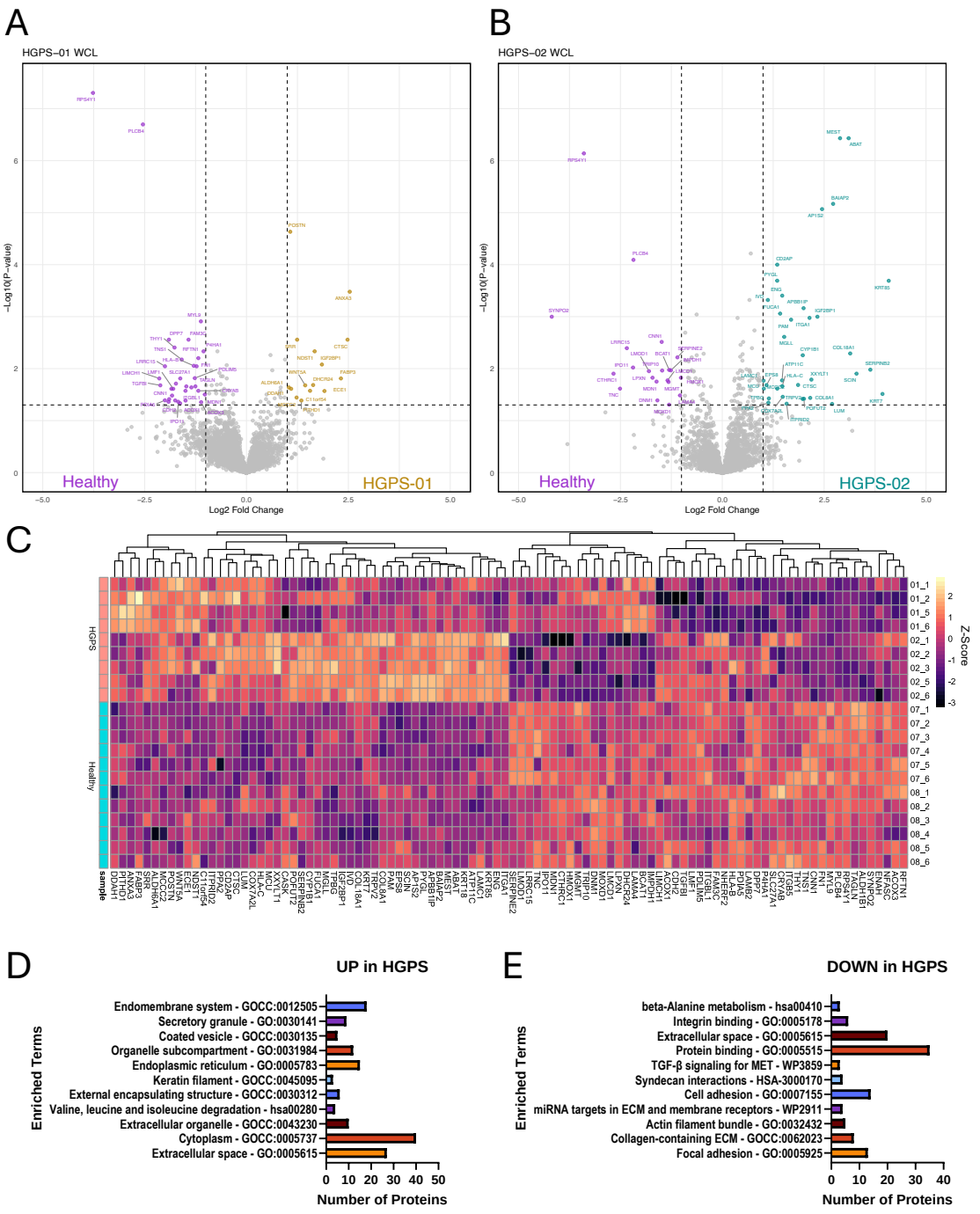

Figure 8: The proteome of HGPS Fibroblasts WCL.

(A) Volcano plot of HGPS-01 and **(B)** HGPS-02 with respect to average data for HC demonstrating differential protein expression. Significance was set at 2-fold change and a p-value of 0.05 **(C)** Heatmap of differentially expressed protein for each patient. The dendrogram was generated following clustering of columns (proteins) using complete linkage clustering and Euclidian distance calculation to reveal patterns in protein expression, while the rows (cells) were not clustered. For cells (row) labeling, 01 and 02 are HGPS while 07 and 08 are healthy cells. The numbers after cell number (e.g., 01-1, 01-5) represent replicate numbers. **(D)** Enrichment analysis of ontology terms upregulated and **(E)** downregulated in HGPS fibroblasts. Enrichment analysis was performed using the STRING App in Cytoscape with redundancy removal set at 0.5. P-values for all terms were all significant at a maximum p-value of 0.01.

Upon closer investigation of specific protein subclasses (keratins) and protein with distinct subcellular localisation (lysosome and mitochondria), datasets appeared to be well normalized. KRT18, which has been shown to be upregulated at the transcriptomic level by others[163], was greatly upregulated in HGPS-02 and trended upwards in HGPS-01 with no change in another basic keratin isoform (KRT9, Figure 9A). β-galactosidase (GLB1) appeared upregulated in HGPS-02, while cathepsin C was increased in HGPS-01 (Figure 9B). Increased β-galactosidase staining is a marker of cellular senescence (SA-β-gal), which has been linked to its increase and accumulation in the lysosome of senescent cells[58]. It is of note, that my proteomic method cannot determine if the increased GLB1 is indeed within the lysosomal compartment. Lastly, changes in mitochondrial protein expression, with structural and enzymatic importance has also been observed (Figure 9C); although, these are not directly related to oxidative phosphorylation which is decreased in HGPS[164]. Differential protein expression was also observed in glutathione S-transferase (GST) proteins and peroxiredoxins, proteins with important roles in the management of oxidative stress (Supplemental Figure 3A). A network-based analysis linked these changes to TP53 (p53), a protein which is important in senescence and NF-κB, however, these proteins were not quantified, potentially due to low abundance. Overall, I have identified protein dysregulation that is consistent with previously reported changes in HGPS, along with some novel differences, thus, my dataset may be useful for an integrative analysis with EV proteomic data.

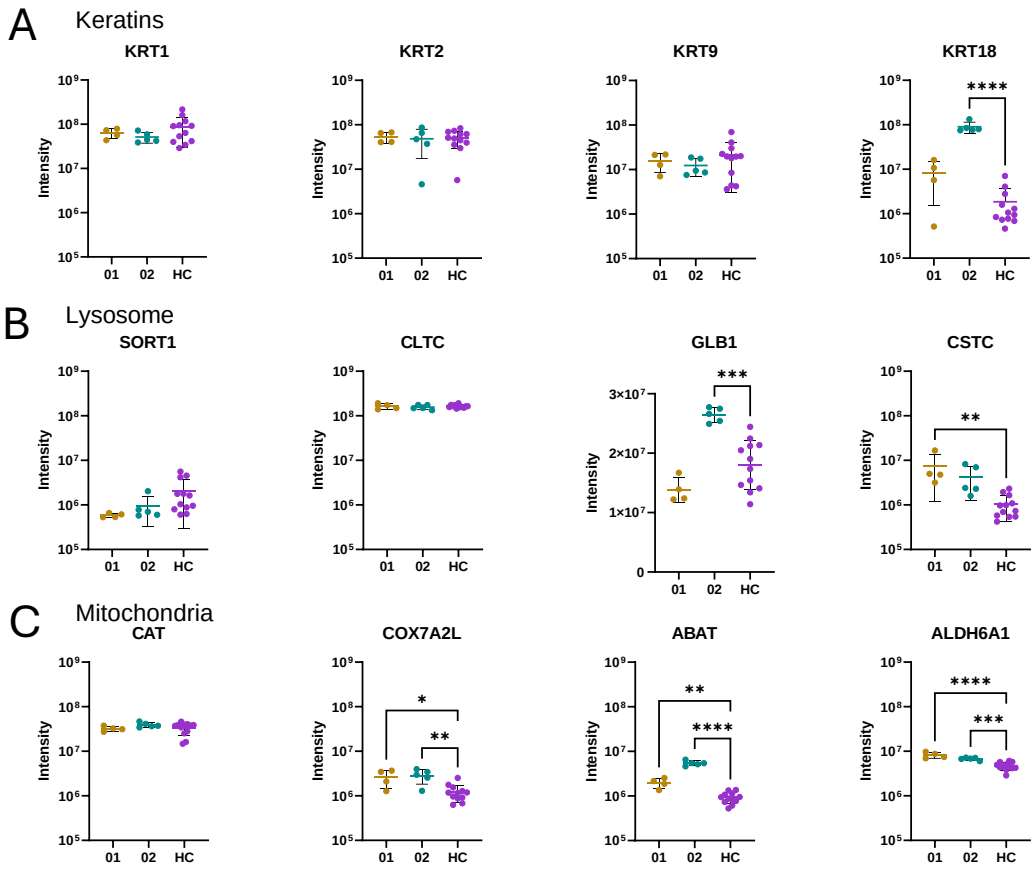

Figure 9: Examples of protein quantification in HGPS fibroblasts.

(A) KRT18 is upregulated, while other acid and basic keratins remain unchanged. **(B)** Lysosomal GLB1 and CSTC are upregulated in specific HGPS patients. **(C)** Many mitochondrial proteins with various functions are consistently upregulated in each HGPS patient. Each point is one independent biological replicate. Statistical significance was computed using a one-way ANOVA comparing HGPS patients against HC, with Dunnett's post-hoc test for multiple comparisons. Only significant p-values <0.05 were graphed. Statistical significance is indicated as * p<0.05, ** p<0.01, ***p<0.001, **** p<0.0001.

4.3.2. The Proteome of HGPS extracellular vesicles.

As I gained an understanding of the protein landscape within HGPS fibroblasts, I then investigated the proteome of HGPS fibroblast-derived EVs in comparison to HC. To do this, UF-SEC fractions were individually digested as optimized above, pooled, and run on an Orbitrap Eclipse operating in the DIA mode. All file processing occurred using the largest spectral library produced above.

The overall proteome of the HGPS EVs was found to contain 1586 proteins. There were few proteins with differential expression, and most of these significant proteins were different between the two HGPS patients (Figure 10A and B). EFR3A, a protein that regulates phosphatidylinositol 4-phosphate was downregulated in HGPS-01. CLPTM1 was also downregulated and has been identified as a lipid scramblase. HGPS-02 expressed less CEMPI2, a protein with hyaluronidase activity, with respect to HC. These results suggest that these HGPS EVs may be interacting with their extracellular environment differently, as there appears to be dysregulation in lipid membrane metabolic processes. No HGPS EV lipidomic studies have been reported to date in the literature.

A significantly larger number of proteins were found to be upregulated in both HGPS cell lines (Figure 10A and B). HGPS-02 had upregulated amyloid-precursor and amyloid precursor-like 1 protein (APP and APLP1), proteins involved in extracellular amyloid plaque formation in neurodegenerative diseases. However, this is a pathology that is unreported in HGPS[165]. Netrin-4 (NTN-4), a protein previously correlated with increased immune infiltration in breast cancer, was also upregulated[166]. Serglycin (SRGN), a protein which is strongly linked to pro-inflammatory environments in brain and tumor microenvironments was also found to be upregulated in HGPS-02[167,168].

Overall, there was notable representation of proteasome and ribosomal proteins (Figure 10C). The identification of proteins annotated with the MVB subcellular localization may suggest that a specific subpopulation of these EVs may be exosomes. Indeed, upon further investigation into the data, at the fraction-wise level, reveals a peak of MVB protein in fraction 8.

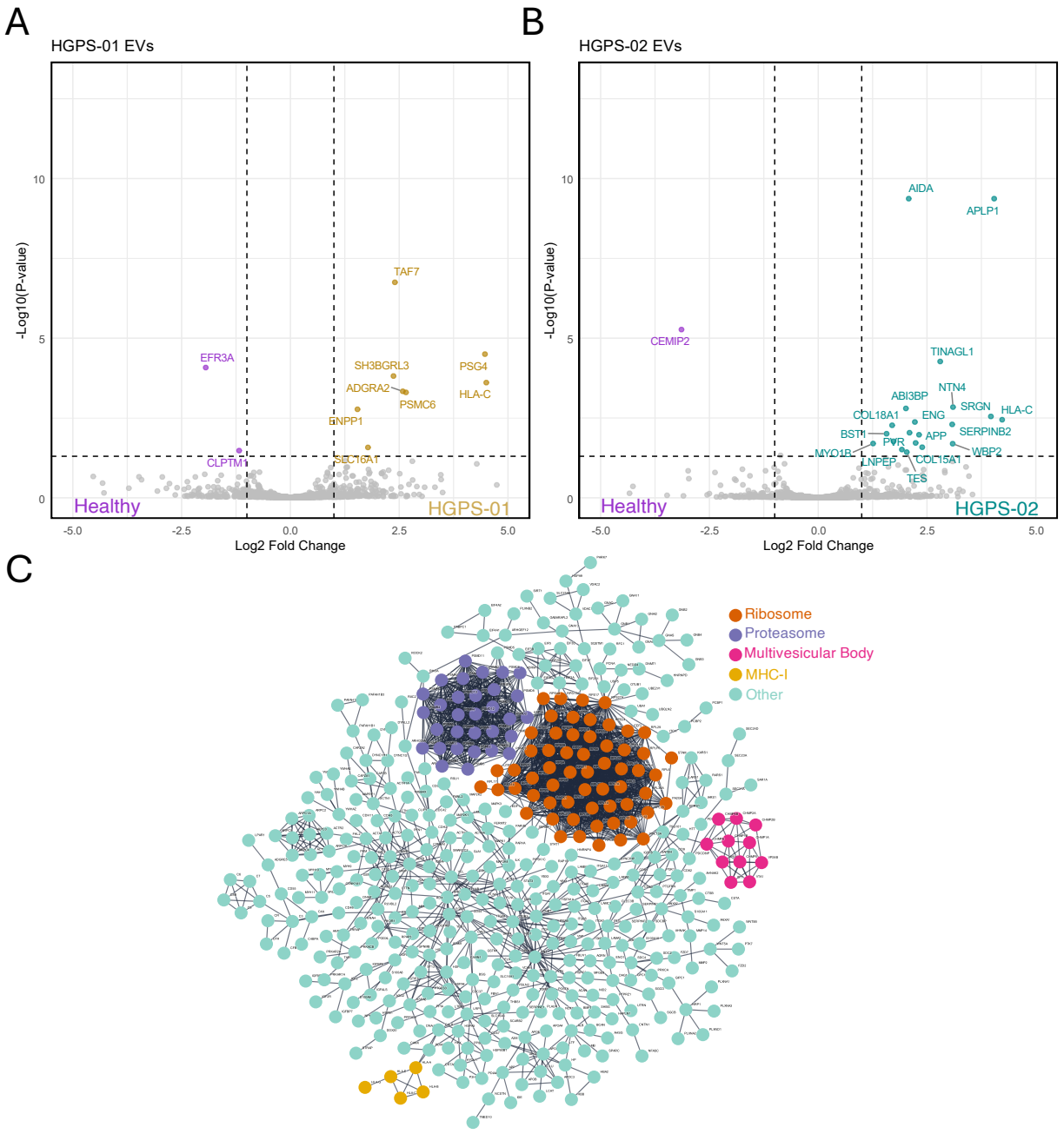

Figure 10: The proteome of HGPS EVs.

(A) Volcano plot of fibroblast-derived EVs from HGPS-01. **(B)** Volcano plot of fibroblast-derived EVs from HGPS-02. Significant protein, defined using a 2-fold change and adjusted p-value threshold of at least 0.05, are labeled. **(C)** Physical protein interaction (PPI) network generated in the STRING app, within Cytoscape. All 1586 proteins identified in the pooled PCV were imported into Cytoscape, with PPI confidence of 0.95. The final network contains 460 nodes (protein) and 2282 edges (interactions), representing the largest subnetwork, to reduce graphical burden.

4.4. Key findings from the HGPS proteome

4.4.1. Integration of HGPS WCL and EV proteomics data to identify proteins of interest

Multiomic data integration has been an area of active research in recent years due to the democratization of omics technology, data workflow, and data availability. Another important factor has been the push towards a systems understanding of biology. The data collected in my project is the most amendable to horizontal integration or homogeneous meta-analysis, that is combining data from the same type of biomolecule[169]. Traditionally this sort of method would rely on data collected using different enrichment methods such as phospho- and acetyl-proteomics, however, my methods enriches two distinct fractions, cellular protein (WCL) and extracellular vesicle protein (EV).

My first attempt at integration was using a ratio-based approach, by comparing fold-changes of proteins identified in both the WCL and EV datasets, regardless of individual significance levels. As expected from the previous data collected in this study (Figure 8C,10A and B), HLA-C was upregulated in both datasets (Figure 11A and B). This analysis produced 4 distinct groups of proteins, upregulated and downregulated in both WCL and EVs, and two groups where the direction of change in WCL and EVs is discordant. Interesting subsets of protein were identified, specifically related to immune function. To further facilitate data interpretation and generalization, average fold-changes for WCLs and EVs were computed (Figure 11C), this removes proteins which shows discordance in fold change directions, which were generally small in the initial analysis and may not be the best representation of altered protein expression in HGPS. Following this manipulation, HLA-C remained significant, along with proteins such as CD9 which is an EV marker and has been previously linked in inflammation[170].

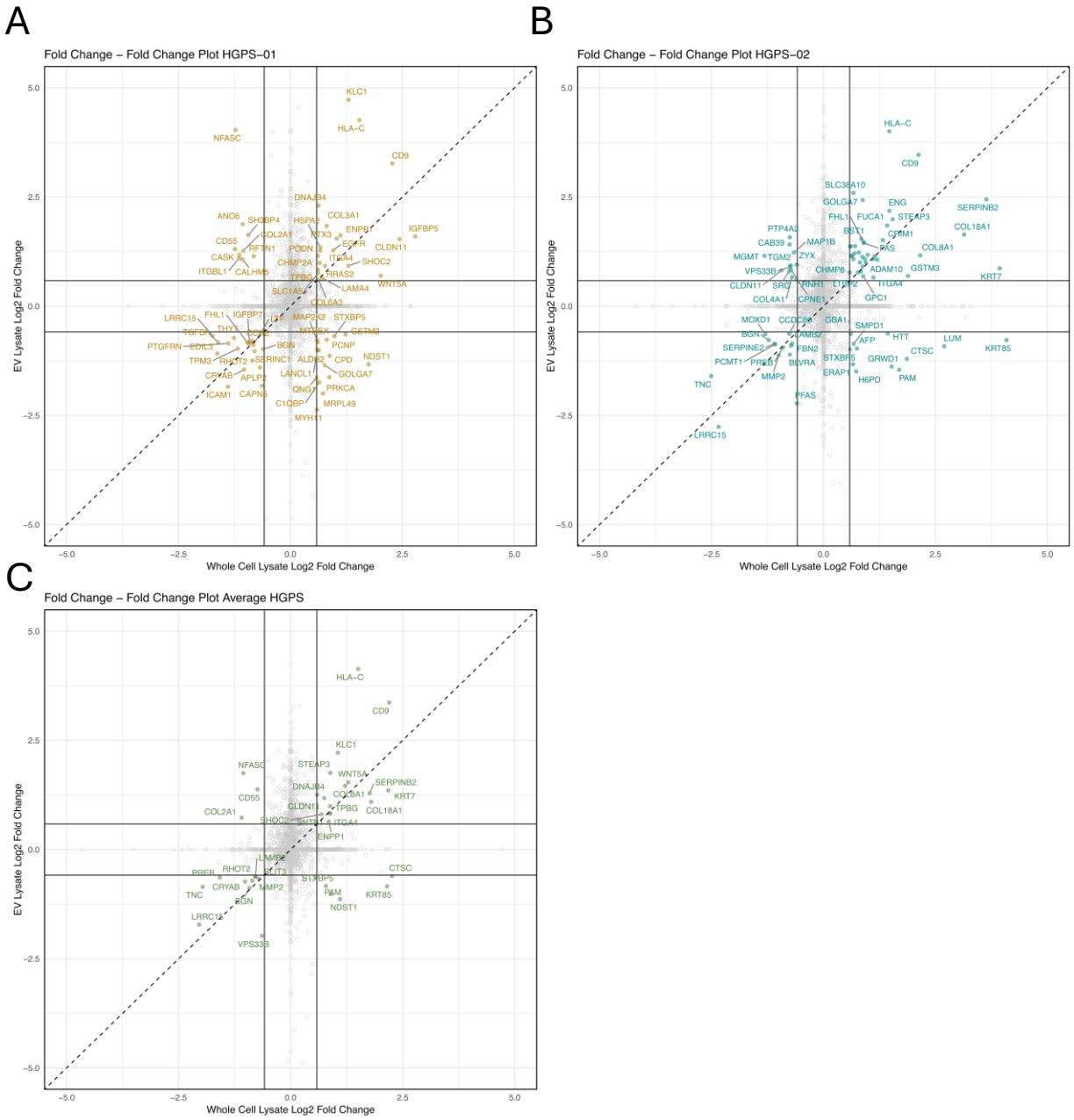

Figure 11: Horizontal multiproteomic data integration reveals protein targets common to HGPS fibroblasts and HGPS EVs.

(A) Fold change plot of HGPS-01 WCLs and EVs . **(B)** Fold change plot of HGPS-02 WCLs and EVs. **(C)** Average fold-changes were computed for both groups in A and B, then plotted again to reduce the number of proteins, biasing towards protein which move in the same direction while reducing the number of proteins with discordant expression in each dataset.

4.4.2. HLA-C is upregulated in HGPS WCL and EVs

Manual validation of the MHC-I class peptides in both WCL (Figure 12A) and EVs (Figure 12B) using the Skyline platform confirmed upregulation of HLA-C, and no differential expression in other HLA paralogs. HLA-G appeared upregulation in HGPS-02, but the potential for statistical significance was lost as the peptides were not detected in half of the samples. The associated light chain for MHC-I, β2M, demonstrated little differences in HGPS when compared to HC. Similarly, HLA-C and G appeared upregulated in HGPS fibroblast-derived EVs. All peptides used to quantify HLA-C were extracellular, but did not contain the N-linked glycosylation site, which is important for protein localization. Glycosylation analysis of the N-linked peptide was not performed. As the MHC-I locus contains many HLA paralogs, each with individual alleles that vary between individuals, the exact allele is important in the study of MHC-I protein. No previous data has been generated about the specific alleles of our patient derived samples, and this was unassessed by our mass spectrometric methods. Others have reported upregulation of many MHC-I protein in chemotherapeutic agent-induced cancer cell senescence, using immunochemical methods which target HLA-A/B/C, but no methods targeting a single paralog[171,172]. A PRM assessment of HLA-C, and other MHC-I proteins produced the same results. Initial data from a male HGPS patient of black descent also demonstrated patent upregulation in EV-associated HLA-C , which may suggest that HLA-C upregulation is intrinsic to HGPS (data not shown).

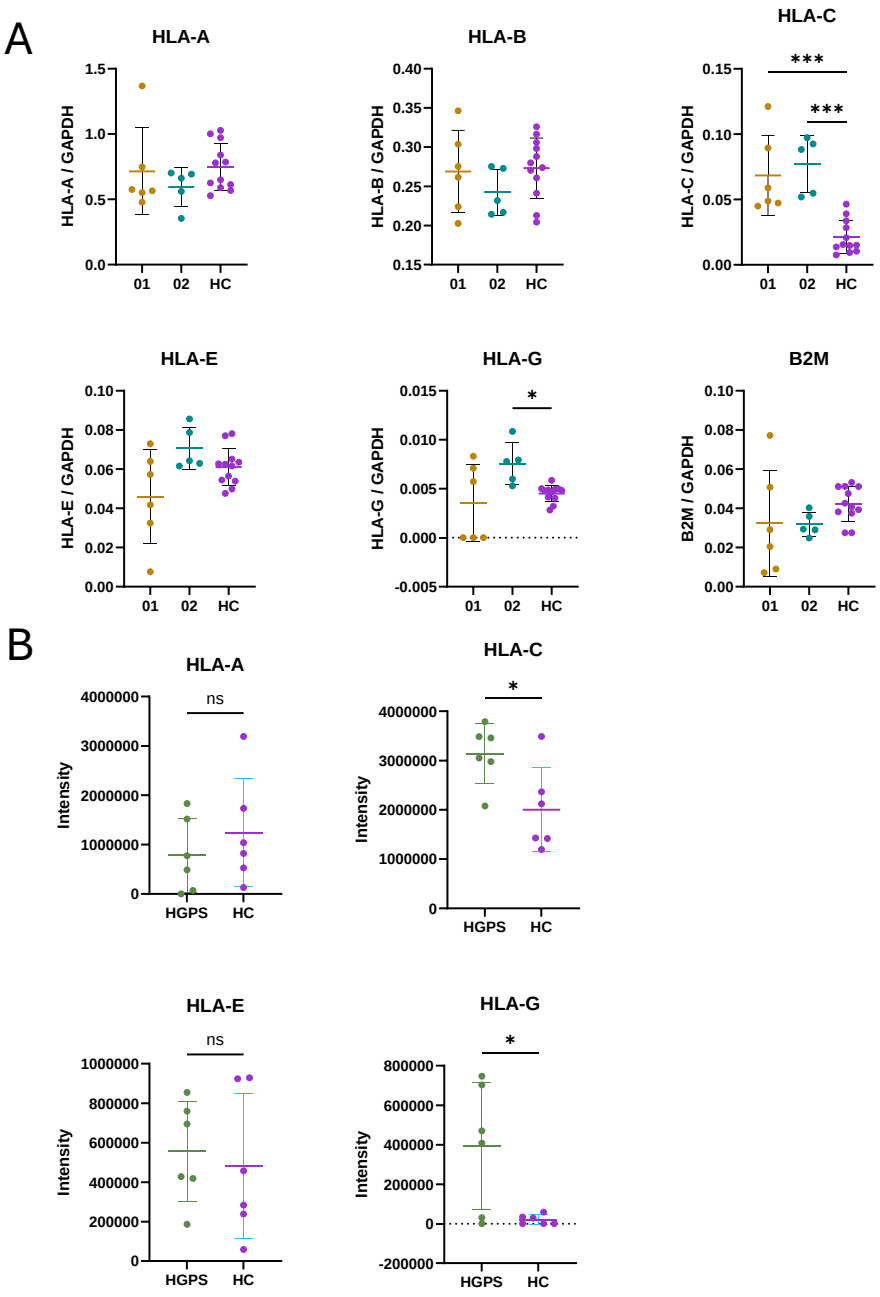

Figure 12: Upregulation in HLA-C is consistent in WCL and EVs.

(A) HLA-C is upregulated in HGPS WCL, while HLA-G, appears upregulated in HGPS-2. No differential expression is observed in other MHC-I paralogs or β2M light chain. A one-way ANOVA was used to compute p-values; insignificant p-values are not shown. **(B)** HLA-C and HLA-G appear upregulated in HGPS EV lysates from fraction 6-9 (inclusive). Fraction 10 was unassessed due to poor peak quality, likely due to low abundance. The student's t-test was used to compute p-values. Manual validation was performed in Skyline.

5. DISCUSSION

5.1. An optimized method for EV isolation from HGPS fibroblasts.

As EVs have gained traction across many subfields in biomedical science, as biomarkers, therapeutic delivery vehicles or as mediators of disease spread, many researchers are increasingly interested in purifying EVs from different sources. Since the identification of "platelet dust" almost 80 years ago, a plethora of methods have been developed for EV isolation [103]. A key first step is the removal of cells and cellular debris, generally achieved through centrifugation; from this point, numerous methodologies exist. When designing an EV experiment, researchers must consider their endpoint analyses and intended applications, such as transcriptomics, proteomics, immunoblotting, intact vesicle immunolabelling, co-culture or *in vivo* experiments such as adoptive transfer of EVs, and vesicle bioprinting[173,174]. Many studies comparing EV isolation methods emphasize the biological sample used as the source material, such as plasma or cell culture media[175,176]. Each combination of sample type and endpoint analysis presents unique challenges, for example, the limited availability of donor biofluids from biobanks[176], or the stringent purity requirements for therapeutic EVs.

In this project, I investigated the proteomic landscape of HGPS fibroblast-derived EVs grown in cell culture, containing FBS. While preparing for this study, I optimized my EV isolation approach by drawing inspiration from cell culture-derived and blood-derived EV isolation methods to minimize FBS contamination before LC-MS/MS analysis. I chose not to use serum depletion kits, as some studies have reported the loss of certain EV markers following this step, potentially suggesting the loss of EVs or certain EV subpopulations, depending on the identity of the specific markers which are lost[177]. This is exemplified by a study by Reymond and colleagues, which tested the High Select ™ Top 14 Abundant Protein Depletion Columns from Thermo Scientific, which

documented a reduction in EV markers, despite increases in particle concentration measured by NTA and number of identified protein by mass spectrometry following a second round of purification by Izon qEVsingle 70nm columns[177]. To enhance sample purity, I compared three isolation methods namely, SEC, UC and UF-SEC, based on the literature and unpublished data from our laboratory. At each step, the yield of protein IDs increased approximately 2-fold, alongside improvements in manual protein identification from MS data.

Pre-concentration of EVs appeared to enrich for smaller particles, causing the particle size distribution to deviate from the generally accepted log-normal distribution[178,179]. These smaller particles may not be EVs, but rather NVEPs, such as exomeres or supermeres which are gaining attention in secretome research. To mitigate potential NVEP contamination in purified EVs, the SEC method presented here was carefully designed. The PCV was judiciously selected to exclude the peak of NVEP markers in fraction 12. A potential adaptation of this method to further isolate NVEPs would be using immune-isolation using known components of these multimolecular assemblies such as lactate dehydrogenase A and B (LDHA / LDHB), or amyloid precursor protein (APP), however, as relatively little is known about the structural organization of these particles, this method may be limited[158]. Otherwise, subjecting fraction 12 to asymmetric-flow field-flow fractionation (AF4) or UC which were techniques initially used to isolate these particles[157,158]. Of note, AF4 demonstrates superior resolution when compared to SEC in multiple use cases, however, no comparison was found in the literature specifically regarding EVs or NVEPs[180,181].

Significance and Impact. The method presented in this thesis allows for the separation of abundant serum proteins from EVs, in a matrix which contains high amounts of FBS. This may open the possibility of collecting EVs from CM, in contexts where serum depletion is not recommended or will decrease the yield in the particles of interest. Indeed, this method is useful

to our laboratory, to test the effects of other stressors on EV production and molecular signatures, without the confounding effects of serum starvation. Our methods differs from others, which apply UF, followed by SEC, then concentrate fractions with UF (a UF-SEC-UF workflow) or SEC-UF, which increase processing time, consumables and may induce increased sample losses[182,183]. While I claim my method is optimal, there is room for further improvements, particularly to remove more FBS proteins, or phenol red. Further adaptation of this method to assess NVEPs, such as exomeres or supermeres, with a focus on fraction 12, may be meritorious as diversity in the current methods to isolate these particles with emerging biological relevance is lacking[157].

5.2. Proteomics for EV characterization.

The final coverage of the human proteome within the HGPS EVs following the analysis of 6 biological replicates was found to include 1,464 unique human proteins (exclusive of proteins which were also identified in FBS), representing approximately 8% of the human proteome and 30% of the proteins in the spectral library, which defines the maximum number of identifiable proteins in this study. This proportion may seem large when compared to the cellular proteome. However, a 2017 Vesiclepedia dataset includes over 13,000 unique proteins identified in human EVs using various mass spectrometric technologies, with some protein validated through orthogonal methods such as immunoblot, antibody arrays or flow-assisted cell sorting[109]. Up to 153 protein IDs that were identified are likely contaminants due to the FBS proteome and tryptic peptide sequence similarities between human and bovine proteins, despite the exclusion of non-unique (razor) proteins[184].

Our proteomic analysis has revealed 82 mitochondrial proteins when searching my dataset against the human MitoCarta database, suggesting that our preparations may contain mitovesicles, which have been previously identified as being important damage-associated molecular pattern

(DAMP) shuttles capable of inducing inflammation[185,186]. However, there were no significantly dysregulated mitochondrial proteins in our HGPS EVs with respect to HC. The nuclear lamina protein LMNA, which is mutated in most HGPS cases to form progerin following enzymatic processing, was also found within our EV preparations. However, the specific peptides identified were common to LMNA and progerin. Interestingly, plasma-derived progerin has been used as a biomarker for clinical immunoassays as an outcome to measure the efficacy of HGPS therapeutics, particularly Lonafarnib in clinical trials[187]. Given that LMNA levels in the plasma of healthy individuals are not thought to exceed 6.8 ng/mL, while plasma progerin of HGPS patients can exceed 33 ng/mL, it is plausible that EVs stabilize extracellular progerin in HGPS, supporting its use as a biomarker[187,188]. However, due to the significant cellular stresses associated with HGPS, increased cell death, in tissues such as smooth muscle, is likely an important contributor to the high levels of plasma progerin that is observed in patients[189].

Proteomic results of EVs lacked growth factors and classical SASP markers such as cytokines and chemokines. This is, partially expected as these proteins tend to be small, and thus produce few tryptic peptides for analysis by LC-MS/MS; these proteins in non-EV bound forms are expected to elute in later SEC fractions. Identification of these proteins could have been a direct link to inflammaging, as mentioned above, and EVs have been found to stabilize these factors on their surfaces and within their lumens[190]. The utilization of immunodetection methods, such as enzyme linked immunosorbent assay (ELISA) may improve the detection of these proteins. Other proteins that are strongly linked to HGPS, such as p53 or CDKs were not identified in our study of these EVs.

Significance and Impact. Proteomic analysis of EVs is a powerful tool, allowing researchers to identify the protein landscape of these particles, which may have profound implications on the

bioactive properties. My MS method, coupled with EV isolation, has given me an unprecedented view into the HGPS secretome, by assessing individual and pooled EV fractions. To date, the secretome of HGPS fibroblasts has been assessed by ELISA for the hallmark SASP molecules such as IL-1β and IL-18[86]. My method of investigating EV cargo, though time-consuming, has resulted in deep-proteome coverage which is sometimes lacking in other MS-based assessment of EVs. The mass spectrometric results of these EVs may provide novel insights into HGPS disease biomarkers for use in clinical trials involving HGPS patient outcomes, while this project focused on the identification of EV-associated proteins which may be implicated in inflammaging.

5.3. Key EV proteins in HGPS potentially implicated in inflammaging.

My optimized EV isolation and proteomic methods have produced an unrivaled understanding of the EVs produced in HGPS. When analyzing dysregulated proteins within the HGPS EVs, particularly in HGPS-02, an interesting protein-protein interaction emerges. HLA-C and Leucyl and cysteinyl aminopeptidase (LNPEP, also known as insulin regulated aminopeptidase [IRAP]) have been identified to interact in the early endosomal compartment of cells, which promotes peptide antigen processing and loading onto HLA-C[191]. This process occurs prior to the formation of the mature HLA-C-β2M heterodimer formation and its subsequent presentation on the cell surface[191]. The presence of MHC-I on EVs is well established, however, the consistent upregulation of HLA-C in both WCL and EVs across the HGPS patient samples analyzed in this thesis is notable. This finding may offer insights into the disease state of HGPS, as a 2020 report suggested that LNPEP promotes inflammatory gene expression by activating NF-κB pathway; and has been previously implicated in psoriasis, a chronic inflammatory disease [192,193].

HLA class I is expressed by all nucleated cells and plays an important role in self-recognition by presenting processed intracellular peptides as antigens to the immune system. Basal HLA

expression varies between cell types and genotypes and can be upregulated in response to pro-inflammatory stimuli[194,195]. Much of the research related to MHC-I expression originates from transplant immunology, where mismatched HLA alleles can significantly impact organ rejection and clinical outcomes[196]. In C2C12 myoblasts, activation of the NLRP3 inflammasome following a challenge with lipopolysaccharide (LPS) and adenosine triphosphate (ATP) has been shown to induce upregulation of MHC-I, an effect that was mitigated by the NLRP3 inflammasome inhibitor MCC950[197]. Notably, a previous study has demonstrated upregulation of NLRP3 in HGPS[86]. However, establishing a direct link between NLRP3 and HLA-C in this context is challenging, as many studies rely on antibody-based techniques that are MHC-I paralog-agnostic. While HLA-C may be involved in several complex immunological pathways related to intrinsic defects in HGPS, no experimental efforts were made to connect these pathways, *in silico* interactomics could not be performed as NLRP3 was not detected in our proteomic data, possibly due to low expression levels. Such an analysis remains an interesting area of further investigation.

Another key aspect of the HGPS pathology is DNA damage, particularly dsDNA breaks which are often visualized experimentally using γH2AX staining. A key cytosolic sensor of dsDNA breaks is the cGAS-STING pathway, which can lead to AIM2 inflammasome activation. Recently, hormonally active vitamin D was found to attenuate cGAS-STING responses in HGPS[198]. Interestingly, in cancer, MHC-I expression was found to be upregulated through a feedforward mechanism involving dsDNA breakage, activation of the cGAS-STING pathway, intracellular transfer of cyclic GMP-AMP (cGAMP) between cells and interferon signaling[199]. This raises the possibility that the HLA-C regulation observed in this thesis may be due to dsDNA damage and a similar feedforward mechanism between senescent and replicating cell populations in culture. However, despite mild STING1 upregulation in HGPS WCL, no components of the cGAS-STING

pathway capable of driving a feedforward mechanism were detected in our EVs. While EV-mediated transfer of these components has been suggested, it has yet to be experimentally validated[200]. Using knowledge from the relevant literature, and my experimental data collected during this project, I propose a working mechanistic hypothesis where upregulation of cGAS-STING activation in response to DNA damage and mis-localized DNA leads to upregulation of HLA-C, which presents itself on the cell surface and/or within the endomembrane system. These compartments allow for the shedding of EVs, with high amounts of HLA-C, which may function to reduce immune cell activation, and potentially reduce the clearance of senescence cells. This is schematically demonstrated in Figure 13.

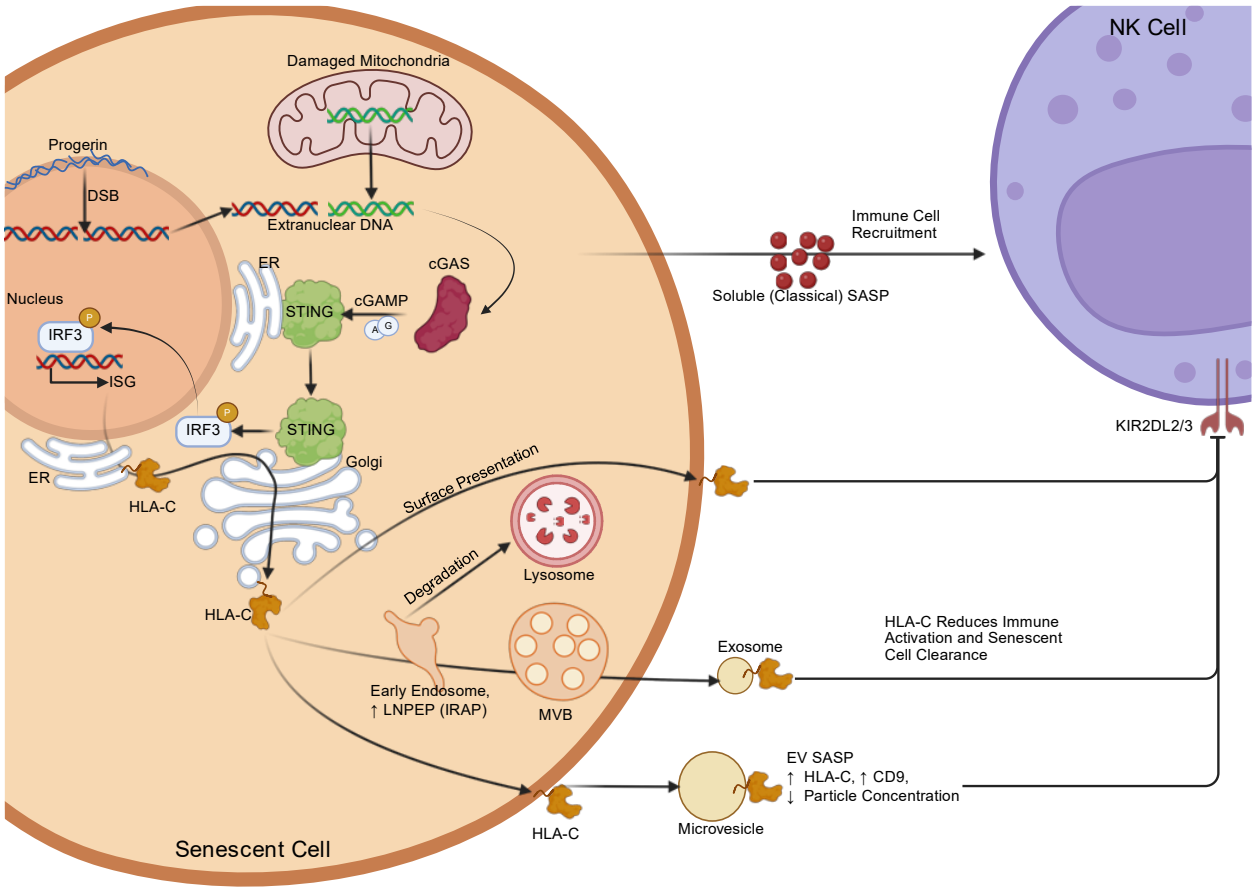

Figure 13: Working Mechanistic Hypothesis of HLA-C Upregulation in HGPS

(A) HLA-C is upregulated in HGPS WCL and EVs with respect to HC. As HGPS fibroblasts are known to have greater amounts of DNA damage and mis-localization, activation of cGAS-STING in the disease has been established. In this study, I was able to identify novel upregulation of HLA-C in these cells, which is itself part of the Interferon Stimulated Genes (ISG). HGPS fibroblasts may be demonstrating an interferon-like response to this damaged DNA, particularly mitochondrial DNA. The classical SASP served as a potent signal for immune cell recruitment and activation, however, HLA-C on the HGPS cell surface, EV surface or within EVs may serve as signals to reduce immune cell activation, in turn reducing senescent cell clearance.

Proteins involved in redox homeostasis have been identified in EVs in multiple other studies. I have observed dysregulation of GST and peroxiredoxin proteins in WCL (Supplemental Figure 3), though this was less evident to observe in EVs. However, in the context of diseases, HGPS is characterized by significant oxidative stress and DNA damage. It is plausible that HGPS fibroblasts are sequestering GST enzymes within the intracellular compartment, to mitigate the increased burden of oxidative stress. In support of this hypothesis, a 2020 study found that EVs derived from aged fibroblast donors exhibited reduced GST activity[201].

Significance and Impact. This study has identified many proteins related to the pathological mechanism of HGPS, and some proteins which have never been reported or examined in the context of the disease. HLA-C, due to its ability to be localized on the cell surface while displaying peptide antigens, is interesting to identify within the HGPS EVs. More importantly, the validated upregulation of this protein has thrust it to the forefront of derivative projects from this thesis in the lab. More generally, the potential linkage of HLA-C to another disease process may increase general interest in this protein, which is mostly understood in the context of placentation and pregnancy. Together with work form others about HLA-E, MHC-I may become an important set of proteins for future study in the context of senescence and inflammaging.

5.4. Limitations of this study

The work presented in this thesis has important limitations that should be addressed. The first concerns sex-differences between the HGPS and HC, as all HGPS patients in this study are female. There are no reported differences in HGPS incidence between sexes[81]. Extensive evidence demonstrates sex-differences for *in vivo* experiments, where factors such as steroid signaling, increased female genetic mosaicism and anatomical differences play important roles[202,203]. Research involving patient-derived EVs from biofluids has identified some instances of sex-based

differences, however, key characteristics such as size distributions, EV yield, and protein and RNA content appear to be largely unaffected[204]. Notably, there is evidence of sex-based differences for specific molecules, most notably miRs[204,205].

In cell culture experiments, the importance of sex as a biological variable is widely recognized. Studies involving primary mouse cells have demonstrated sex-dependent differences in gene expression and cell death sensitivity based on sex[206] Similarly, in human models, such as induced pluripotent stem cells derived from fibroblasts to generate blood-brain barrier models, sex-differences have again been shown to be an important factor[207]. To account for these limitations, lists of proteins identified by MS were cross-referenced against databases containing sex as a metadata variable[208,209]. However, analysis using the sex differences in Cancer Database was unsuccessful due to data inaccessibility[210]. Importantly, this analysis did not exclude HLA-C from our results. Currently, no comprehensive database exists cataloging differential protein content as a function of sex, only reviews summarizing key findings from subsets of published research[204]. While the creation of such a database was beyond the scope of this project, it remains an interesting area of future research, particularly as EVs continue to advance in theranostics and as the MISEV Consortium works toward standardizing EV research worldwide[107,211]. Another potentially significant variable in the biologically male HC cells is whether the Y chromosome remains intact or has been lost, a phenomenon reported in other studies following serial passaging and culturing of immortal cell lines, particularly in cancer research[212]. A second key limitation, particularly regarding patient profiles, is the lack of racial and genetic diversity. All four patient-derived samples used in this thesis were from individuals classified as white, according to Corriell Institute documentation. While racial differences are primarily associated with variations in molecular cargo rather than EV size and concentration[204,213], this limitation may affect the generalizability of

the findings to non-white HGPS populations. Although HGPS has been reported across diverse ethnic backgrounds, publication bias has been suggested as a factor contributing to the predominance of Caucasian cases in the literature[214]. Preliminary, unpresented data from an HGPS donor with a black background appears to be consistent with the major findings of this thesis, specifically with respect to HLA-C. The ability of this study to draw significant results may be limited due to the small sample size of patients included in our analysis, which is common in studies of rare diseases. In a future follow-up study, special attention should be given to increasing the number of patient-derived fibroblast or other cell lines used, which would allow the research group to tease out with greater confidence disease-specific modifications that are common between many HGPS patient EVs.

In this project, I have determined that DIA with spectral library, is the optimal method for the identification of proteins in UF-SEC fractions. Some studies suggest that DDA experiments, using identification and quantification from spectral libraries provides results similar to those of obtained with DIA [215]. However, the processing of DDA data with spectral libraries was not attempted in this project, as I chose to follow classical sequence database-based identification and quantification methods. Nonetheless, it is worth noting that when considering manual data validation using tools like Skyline, DIA provides a distinct advantage. MS2 spectra should be present for all m/z ratios within user-defined isolation windows, regardless of precursor ion intensity[140]. In practice, this allows the human validator to have increased confidence in the true missingness of a particular peptide. Regarding spectral libraries, this project did not employ in *silico* predicted or theoretical spectral libraries, which have gained popularity in recent years due to the advancements in machine learning and deep learning technologies[216,217]. These technical limitations remain an interesting avenue for future improvement.

HLA-C, despite its significant role in immunology, remains relatively poorly characterized beyond the maternal-fetal interface. The existing body of evidence suggests that extracellular, antigen-presenting HLA-C plays a crucial role in the immune response. Whie HLA-C is highlighted as an important protein in this thesis, I lack evidence to support its specific localization within the cell or whether it is embedded in the membrane of the EVs, which is critical for its function. This may be achieved using nano flow-cytometry of EVs labeled with fluorescent anti-HLA-C antibodies or by immunogold labeling followed by electron microscopy, or by performing surface proteomics experiments such as hydrazide capture as HLA-C contains an N-linked (asparagine-linked) glycosylation site[218]. In addition, the expression and localization of HLA-C, on the cell surface are influenced by the specific genotype of the biological sample, although it demonstrates less polymorphism compared to HLA-A and HLA-B[219]. Specific MHC-I genotyping was not performed by myself, or by others who have historically used these cell lines, making it impossible to exclude the possibility that both HGPS cell lines carry high-expression HLA-C alleles, while the HC express relatively low-expression alleles[219]. However, there was good agreement in the MS2 fragmentation pattern between all cell lines tested, which may suggest that the specific peptides used to quantify HLA-C in this project are present in cell lines.

6. CONCLUSIONS AND FUTURE PERSPECTIVES

Global populations are aging, presenting a significant challenge for healthcare systems moving forward. Despite considerable investment in aging research, our understanding of the contribution of EVs, potent mediators of paracrine and endocrine intercellular communication, remain limited. Furthermore, although rare diseases are individually uncommon when aggregated together, they affect 1 in 12 Canadians, highlighting the need for focused research [220]. Recent evidence showing progerin accumulation within the cells of older adults, comprising up to 1% of LMNA content, underscores the importance of studying rare diseases and their potential relevance to broader populations[221].

Given the complexity of the sample matrix, which contained high amounts of FBS due to the nature of the biological sample, I optimized a hybrid method, consisting of a UF pre-concentration step followed by SEC for isolating EVs using established techniques from the EV literature[222]. However, there is still room to further refine this methodology, potentially by way of immunoisolation of specific EV subpopulations, in fractions which likely contain multiple populations of EVs and NVEPs. To further enhance the proteomic data, DIA and DDA mass spectrometric methods were compared, to maximize the reproducible quantitation of EV proteins. This thesis characterizes the proteome of HGPS fibroblast, and using this knowledge in the form of spectral libraries, explores the proteome of HGPS fibroblast-derived EVs with DIA-MS. Inspired by multi-omic data analysis strategies, I applied a novel approach to HGPS, enabling the identification of a previously uncharacterized protein dysregulation in HGPS EVs, particularly concerning the MHC-I class protein HLA-C. This project begins to explore the role of inflammaging and immunity in non-myeloid HGPS cells, extending beyond the AIM2 and NLRP3 inflammasomes. Given HLA-C's role as a critical immune cell regulator, these results could have profound implications for the clearance of senescent cells, the senescent microenvironment, and

may identify HLA-C as a potential target for senotherapy or anti-inflammaging strategies, which has been suggested for other HLA paralogs. Future investigation of the specific localization of these HLA-C molecules within the EVs, their peptide antigens, and post translational modifications may be of important significance moving forward if the HGPS EVs demonstrate pro-inflammaging bioactivity in cell culture with innate immune or other cell types. While the wider relevance of HLA-C upregulation in physiological inflammaging is still not understood, it appears to be important in HGPS, as a model of advanced chronological old age.

7. REFERENCES

1. Demiris, G. *et al.* High Value Care for Older Adults with Complex Care Needs: Leveraging Nurses as Innovators. *Nurs Outlook* **68**, 26–32 (2020).
2. United Nations. World Population Prospects 2022: Summary of Results. *United Nations Department of Economic and Social Affairs- Population Division* (2022).
3. Garmany, A., Yamada, S. & Terzic, A. Longevity leap: mind the healthspan gap. *NPJ Regen Med* **6**, 57 (2021).
4. Lyu, Y.-X. *et al.* Longevity biotechnology: bridging AI, biomarkers, geroscience and clinical applications for healthy longevity. *Aging (Albany NY)* **16**, 12955–12976 (2024).
5. Finch, C. E. Evolution of the human lifespan and diseases of aging: Roles of infection, inflammation, and nutrition. *Proc Natl Acad Sci U S A* **107**, 1718–1724 (2010).
6. Kaeberlein, M. How healthy is the healthspan concept? *GeroScience* **40**, 361 (2018).
7. Garmany, A. & Terzic, A. Global Healthspan-Lifespan Gaps Among 183 World Health Organization Member States. *JAMA Network Open* **7**, e2450241 (2024).
8. Gold, M. R., Stevenson, D. & Fryback, D. G. HALYS and QALYS and DALYS, Oh My: similarities and differences in summary measures of population Health. *Annu Rev Public Health* **23**, 115–134 (2002).
9. Garmany, A. & Terzic, A. Global Healthspan-Lifespan Gaps Among 183 World Health Organization Member States. *JAMA Netw Open* **7**, e2450241 (2024).
10. *UN Decade of Healthy Ageing: Plan of Action 2021-2030*.
11. Latz, E. & Duewell, P. NLRP3 inflammasome activation in inflammaging. *Seminars in Immunology* **40**, 61–73 (2018).
12. Christ, A., Lauterbach, M. & Latz, E. Western Diet and the Immune System: An Inflammatory Connection. *Immunity* **51**, 794–811 (2019).
13. Prattichizzo, F. *et al.* Inflammageing and metaflammation: The yin and yang of type 2 diabetes. *Ageing Research Reviews* **41**, 1–17 (2018).

14. Qu, L. *et al.* Macrophages at the Crossroad of Meta-Inflammation and Inflammaging. *Genes (Basel)* **13**, 2074 (2022).

15. Crimmins, E. M. Lifespan and Healthspan: Past, Present, and Promise. *Gerontologist* **55**, 901–911 (2015).

16. Franceschi, C. *et al.* Inflamm-aging. An evolutionary perspective on immunosenescence. *Ann N Y Acad Sci* **908**, 244–254 (2000).

17. Finch, C. E. & Crimmins, E. M. Inflammatory exposure and historical changes in human life-spans. *Science* **305**, 1736–1739 (2004).

18. Franceschi, C., Garagnani, P., Parini, P., Giuliani, C. & Santoro, A. Inflammaging: a new immune–metabolic viewpoint for age-related diseases. *Nat Rev Endocrinol* **14**, 576–590 (2018).

19. Varricchi, G., Paolocci, N., Rivellese, F. & Rengo, G. Editorial: Smoldering Inflammation in Cardio-Immune-Metabolic Disorders. *Frontiers in Physiology* **12**, (2021).

20. Coppedè, F. Premature aging syndrome. *Adv Exp Med Biol* **724**, 317–331 (2012).

21. Lowsky, D. J., Olshansky, S. J., Bhattacharya, J. & Goldman, D. P. Heterogeneity in Healthy Aging. *J Gerontol A Biol Sci Med Sci* **69**, 640–649 (2014).

22. Nguyen, Q. D. *et al.* Health Heterogeneity in Older Adults: Exploration in the Canadian Longitudinal Study on Aging. *Journal of the American Geriatrics Society* **69**, 678–687 (2021).

23. Tian, Y. E. *et al.* Heterogeneous aging across multiple organ systems and prediction of chronic disease and mortality. *Nat Med* **29**, 1221–1231 (2023).

24. Yarbro, J. R., Emmons, R. S. & Pence, B. D. Macrophage Immunometabolism and Inflammaging: Roles of Mitochondrial Dysfunction, Cellular Senescence, CD38, and NAD. *Immunometabolism* **2**, e200026 (2020).

25. Giovannini, S. *et al.* Interleukin-6, C-Reactive Protein, Tumor Necrosis Factor-alpha as Predictors of Mortality in Frail, Community-Living Elderly Individuals. *J Am Geriatr Soc* **59**, 1679–1685 (2011).

26. Alberro, A. *et al.* Inflammaging markers characteristic of advanced age show similar levels with frailty and dependency. *Sci Rep* **11**, 4358 (2021).

27. Zhao, H. *et al.* Inflammation and tumor progression: signaling pathways and targeted intervention. *Sig Transduct Target Ther* **6**, 1–46 (2021).

28. Al-Qahtani, A. A., Alhamlan, F. S. & Al-Qahtani, A. A. Pro-Inflammatory and Anti-Inflammatory Interleukins in Infectious Diseases: A Comprehensive Review. *Trop Med Infect Dis* **9**, 13 (2024).

29. Lee, K.-A., Flores, R. R., Jang, I. H., Saathoff, A. & Robbins, P. D. Immune Senescence, Immunosenescence and Aging. *Front Aging* **3**, 900028 (2022).

30. Fuentes, E., Fuentes, M., Alarcón, M. & Palomo, I. Immune System Dysfunction in the Elderly. *An. Acad. Bras. Ciênc.* **89**, 285–299 (2017).

31. Increased number of circulating Leu 11+ (CD 16) large granular lymphocytes and decreased NK activity during human ageing - PubMed. https://pubmed-ncbi-nlm-nih-gov.proxy.bib.uottawa.ca/3498573/.

32. Vitale, M. *et al.* The impairment of natural killer function in the healthy aged is due to a postbinding deficient mechanism. *Cellular Immunology* **145**, 1–10 (1992).

33. Lutz, C. T., Moore, M. B., Bradley, S., Shelton, B. J. & Lutgendorf, S. K. Reciprocal age related change in natural killer cell receptors for MHC class I. *Mechanisms of Ageing and Development* **126**, 722–731 (2005).

34. Gounder, S. S. *et al.* Effect of Aging on NK Cell Population and Their Proliferation at Ex Vivo Culture Condition. *Anal Cell Pathol (Amst)* **2018**, 7871814 (2018).

35. Rukavina, D. *et al.* Age-related decline of perforin expression in human cytotoxic T lymphocytes and natural killer cells. *Blood* **92**, 2410–2420 (1998).

36. Voskoboinik, I., Dunstone, M. A., Baran, K., Whisstock, J. C. & Trapani, J. A. Perforin: structure, function, and role in human immunopathology. *Immunol Rev* **235**, 35–54 (2010).

37. Hazeldine, J., Hampson, P. & Lord, J. M. Reduced release and binding of perforin at the immunological synapse underlies the age-related decline in natural killer cell cytotoxicity. *Aging Cell* **11**, 751–759 (2012).

38. Hazeldine, J. & Lord, J. M. The impact of ageing on natural killer cell function and potential consequences for health in older adults. *Ageing Res Rev* **12**, 1069–1078 (2013).

39. Shehata, H. M., Hoebe, K. & Chougnet, C. A. The aged nonhematopoietic environment impairs natural killer cell maturation and function. *Aging Cell* **14**, 191–199 (2015).

40. Steinmann, G. G., Klaus, B. & Müller-Hermelink, H.-K. The Involution of the Ageing Human Thymic Epithelium is Independent of Puberty. *Scandinavian Journal of Immunology* **22**, 563–575 (1985).

41. Hale, L. P. Histologic and molecular assessment of human thymus. *Ann Diagn Pathol* **8**, 50–60 (2004).

42. Goronzy, J. J., Lee, W.-W. & Weyand, C. M. Aging and T-cell diversity. *Exp Gerontol* **42**, 400–406 (2007).

43. Covre, L. P., De Maeyer, R. P. H., Gomes, D. C. O. & Akbar, A. N. The role of senescent T cells in immunopathology. *Aging Cell* **19**, e13272 (2020).

44. Liu, W. *et al.* Senescent Tumor CD8+ T Cells: Mechanisms of Induction and Challenges to Immunotherapy. *Cancers* **12**, 2828 (2020).

45. Zhao, Y., Shao, Q. & Peng, G. Exhaustion and senescence: two crucial dysfunctional states of T cells in the tumor microenvironment. *Cell Mol Immunol* **17**, 27–35 (2020).

46. López-Otín, C., Blasco, M. A., Partridge, L., Serrano, M. & Kroemer, G. The Hallmarks of Aging. *Cell* **153**, 1194–1217 (2013).

47. López-Otín, C., Blasco, M. A., Partridge, L., Serrano, M. & Kroemer, G. Hallmarks of aging: An expanding universe. *Cell* **186**, 243–278 (2023).

48. Hayflick, L. & Moorhead, P. S. The serial cultivation of human diploid cell strains. *Experimental Cell Research* **25**, 585–621 (1961).

49. Harley, C. B., Futcher, A. B. & Greider, C. W. Telomeres shorten during ageing of human fibroblasts. *Nature* **345**, 458–460 (1990).

50. Bartkova, J. *et al.* Oncogene-induced senescence is part of the tumorigenesis barrier imposed by DNA damage checkpoints. *Nature* **444**, 633–637 (2006).

51. Robert, G. & Wagner, J. R. ROS-Induced DNA Damage as an Underlying Cause of Aging. *Advances in Geriatric Medicine and Research* **4**, (2020).

52. Wu, X., Bayle, J. H., Olson, D. & Levine, A. J. The p53-mdm-2 autoregulatory feedback loop. *Genes Dev* **7**, 1126–1132 (1993).

53. Blackford, A. N. & Jackson, S. P. ATM, ATR, and DNA-PK: The Trinity at the Heart of the DNA Damage Response. *Molecular Cell* **66**, 801–817 (2017).

54. Lee, J.-J. *et al.* HMGB1 orchestrates STING-mediated senescence via TRIM30α modulation in cancer cells. *Cell Death Discov.* **7**, 1–12 (2021).

55. Lv, T. *et al.* Mechanism and role of nuclear laminin B1 in cell senescence and malignant tumors. *Cell Death Discov.* **10**, 1–9 (2024).

56. Kumari, R. & Jat, P. Mechanisms of Cellular Senescence: Cell Cycle Arrest and Senescence Associated Secretory Phenotype. *Front Cell Dev Biol* **9**, 645593 (2021).

57. Kurz, D. J., Decary, S., Hong, Y. & Erusalimsky, J. D. Senescence-associated β-galactosidase reflects an increase in lysosomal mass during replicative ageing of human endothelial cells. *Journal of Cell Science* **113**, 3613–3622 (2000).

58. Lee, B. Y. *et al.* Senescence-associated beta-galactosidase is lysosomal beta-galactosidase. *Aging Cell* **5**, 187–195 (2006).

59. Valieva, Y., Ivanova, E., Fayzullin, A., Kurkov, A. & Igrunkova, A. Senescence-Associated β-Galactosidase Detection in Pathology. *Diagnostics (Basel)* **12**, 2309 (2022).

60. Coppé, J.-P. *et al.* Senescence-associated secretory phenotypes reveal cell-nonautonomous functions of oncogenic RAS and the p53 tumor suppressor. *PLoS Biol* **6**, 2853–2868 (2008).

61. Basisty, N. *et al.* A proteomic atlas of senescence-associated secretomes for aging biomarker development. *PLoS Biol* **18**, e3000599 (2020).

62. Zhang, D. *et al.* Therapy-induced senescent tumor cell-derived extracellular vesicles promote colorectal cancer progression through SERPINE1-mediated NF-κB p65 nuclear translocation. *Molecular Cancer* **23**, 70 (2024).

63. Wallis, R., Mizen, H. & Bishop, C. L. The bright and dark side of extracellular vesicles in the senescence-associated secretory phenotype. *Mech Ageing Dev* **189**, 111263 (2020).

64. Yeh, S. *et al.* Higher senescence associated secretory phenotype and lower defense mediator in urinary extracellular vesicles of elders with and without Parkinson disease. *Sci Rep* **11**, 15783 (2021).

65. Pignolo, R. J., Passos, J. F., Khosla, S., Tchkonia, T. & Kirkland, J. L. Reducing Senescent Cell Burden in Aging and Disease. *Trends Mol Med* **26**, 630–638 (2020).

66. Sagiv, A. & Krizhanovsky, V. Immunosurveillance of senescent cells: the bright side of the senescence program. *Biogerontology* **14**, 617–628 (2013).

67. Salminen, A. Feed-forward regulation between cellular senescence and immunosuppression promotes the aging process and age-related diseases. *Ageing Research Reviews* **67**, 101280 (2021).

68. Pereira, B. I. *et al.* Senescent cells evade immune clearance via HLA-E-mediated NK and CD8+ T cell inhibition. *Nat Commun* **10**, 2387 (2019).

69. Storer, M. *et al.* Senescence Is a Developmental Mechanism that Contributes to Embryonic Growth and Patterning. *Cell* **155**, 1119–1130 (2013).

70. Muñoz-Espín, D. *et al.* Programmed Cell Senescence during Mammalian Embryonic Development. *Cell* **155**, 1104–1118 (2013).

71. Demaria, M. *et al.* An essential role for senescent cells in optimal wound healing through secretion of PDGF-AA. *Dev Cell* **31**, 722–733 (2014).

72. Chia, C. W. *et al.* Age-associated expression of p21and p53 during human wound healing. *Aging Cell* **20**, e13354 (2021).

73. Carrero, D., Soria-Valles, C. & López-Otín, C. Hallmarks of progeroid syndromes: lessons from mice and reprogrammed cells. *Dis Model Mech* **9**, 719–735 (2016).

74. Ahmed, M. S., Ikram, S., Bibi, N. & Mir, A. Hutchinson-Gilford Progeria Syndrome: A Premature Aging Disease. *Mol Neurobiol* **55**, 4417–4427 (2018).

75. Chen, X., Yao, H., Andrés, V., Bergo, M. O. & Kashif, M. Status of treatment strategies for Hutchinson–Gilford progeria syndrome with a focus on prelamin: A posttranslational modification. *Basic Clin Pharmacol Toxicol* **131**, 217–223 (2022).

76. Benedicto, I., Chen, X., Bergo, M. O. & Andrés, V. Progeria: a perspective on potential drug targets and treatment strategies. *Expert Opinion on Therapeutic Targets* **26**, 393–399 (2022).

77. De Sandre-Giovannoli, A. *et al.* Lamin A Truncation in Hutchinson-Gilford Progeria. *Science* **300**, 2055–2055 (2003).

78. Eriksson, M. *et al.* Recurrent de novo point mutations in lamin A cause Hutchinson–Gilford progeria syndrome. *Nature* **423**, 293–298 (2003).

79. Kychygina, A. *et al.* Progerin impairs 3D genome organization and induces fragile telomeres by limiting the dNTP pools. *Sci Rep* **11**, 13195 (2021).

80. Koblan, L. W. *et al.* In vivo base editing rescues Hutchinson–Gilford progeria syndrome in mice. *Nature* **589**, 608–614 (2021).

81. Coppedè, F. The epidemiology of premature aging and associated comorbidities. *Clin Interv Aging* **8**, 1023–1032 (2013).

82. Ding, S. & Shen, C.-Y. Model of human aging: Recent findings on Werner's and Hutchinson-Gilford progeria syndromes. *Clin Interv Aging* **3**, 431–444 (2008).

83. Brassard, J. A., Fekete, N., Garnier, A. & Hoesli, C. A. Hutchinson-Gilford progeria syndrome as a model for vascular aging. *Biogerontology* **17**, 129–145 (2016).

84. Plikus, M. V. *et al.* Fibroblasts: Origins, definitions, and functions in health and disease. *Cell* **184**, 3852–3872 (2021).

85. Sahai, E. *et al.* A framework for advancing our understanding of cancer-associated fibroblasts. *Nat Rev Cancer* **20**, 174–186 (2020).

86. González-Dominguez, A. *et al.* Inhibition of the NLRP3 inflammasome improves lifespan in animal murine model of Hutchinson-Gilford Progeria. *EMBO Mol Med* **13**, e14012 (2021).

87. Osorio, F. G. *et al.* Nuclear lamina defects cause ATM-dependent NF-κB activation and link accelerated aging to a systemic inflammatory response. *Genes Dev.* **26**, 2311–2324 (2012).

88. Gritsenko, A., Green, J. P., Brough, D. & Lopez-Castejon, G. Mechanisms of NLRP3 priming in inflammaging and age related diseases. *Cytokine & Growth Factor Reviews* **55**, 15–25 (2020).

89. Pereira, A. C. *et al.* ER-mitochondria communication is involved in NLRP3 inflammasome activation under stress conditions in the innate immune system. *Cell Mol Life Sci* **79**, 213 (2022).

90. Hughes, M. M. *et al.* Glutathione Transferase Omega-1 Regulates NLRP3 Inflammasome Activation through NEK7 Deglutathionylation. *Cell Rep* **29**, 151-161.e5 (2019).

91. Villa-Bellosta, R. Dietary magnesium supplementation improves lifespan in a mouse model of progeria. *EMBO Mol Med* **12**, e12423 (2020).

92. Xiong, Z. *et al.* Methylene blue alleviates nuclear and mitochondrial abnormalities in progeria. *Aging Cell* **15**, 279–290 (2016).

93. DuBose, A. J. *et al.* Everolimus rescues multiple cellular defects in laminopathy-patient fibroblasts. *Proc Natl Acad Sci U S A* **115**, 4206–4211 (2018).

94. Buzzoni, R. *et al.* Activity and safety of RAD001 (everolimus) in patients affected by biliary tract cancer progressing after prior chemotherapy: a phase II ITMO study. *Ann Oncol* **25**, 1597–1603 (2014).

95. Kohl, N. E. *et al.* Selective inhibition of ras-dependent transformation by a farnesyltransferase inhibitor. *Science* **260**, 1934–1937 (1993).

96. Borthakur, G. *et al.* Pilot study of lonafarnib, a farnesyl transferase inhibitor, in patients with chronic myeloid leukemia in the chronic or accelerated phase that is resistant or refractory to imatinib therapy. *Cancer* **106**, 346–352 (2006).

97. Wong, N. S. & and Morse, M. A. Lonafarnib for cancer and progeria. *Expert Opinion on Investigational Drugs* **21**, 1043–1055 (2012).

98. Kleiner, G., Marcuzzi, A., Campisciano, G. & Crovella, S. Farnesyl and geranylgeranyl transferase inhibitors: an anti-inflammatory effect. Comment to "Inhibition of protein geranylgeranylation and farnesylation protects against graft-versus-host disease via effects on CD4 effector T cells" Haematologica. 2013;98(1):31-40. *Haematologica* **98**, e44–e45 (2013).

99. Dhillon, S. Lonafarnib: First Approval. *Drugs* **81**, 283–289 (2021).

100. Decker, M. L., Chavez, E., Vulto, I. & Lansdorp, P. M. Telomere length in Hutchinson-Gilford progeria syndrome. *Mech Ageing Dev* **130**, 377–383 (2009).

101. Bernardes de Jesus, B. *et al.* The telomerase activator TA-65 elongates short telomeres and increases health span of adult/old mice without increasing cancer incidence. *Aging Cell* **10**, 604–621 (2011).

102. Martínez, P. & Blasco, M. A. Telomere-driven diseases and telomere-targeting therapies. *J Cell Biol* **216**, 875–887 (2017).

103. Wolf, P. The Nature and Significance of Platelet Products in Human Plasma. *British Journal of Haematology* **13**, 269–288 (1967).

104. Aimaletdinov, A. M. & Gomzikova, M. O. Tracking of Extracellular Vesicles' Biodistribution: New Methods and Approaches. *International Journal of Molecular Sciences* **23**, 11312 (2022).

105. Lötvall, J. *et al.* Minimal experimental requirements for definition of extracellular vesicles and their functions: a position statement from the International Society for Extracellular Vesicles. *J Extracell Vesicles* **3**, 10.3402/jev.v3.26913 (2014).

106. Théry, C. *et al.* Minimal information for studies of extracellular vesicles 2018 (MISEV2018): a position statement of the International Society for Extracellular Vesicles and update of the MISEV2014 guidelines. *J Extracell Vesicles* **7**, 1535750 (2018).

107. Welsh, J. A. *et al.* Minimal information for studies of extracellular vesicles (MISEV2023): From basic to advanced approaches. *Journal of Extracellular Vesicles* **13**, e12404 (2024).

108. Keerthikumar, S. *et al.* ExoCarta: A Web-Based Compendium of Exosomal Cargo. *Journal of Molecular Biology* **428**, 688–692 (2016).

109. Chitti, S. V. *et al.* Vesiclepedia 2024: an extracellular vesicles and extracellular particles repository. *Nucleic Acids Research* **52**, D1694–D1698 (2024).

110. Zhang, Y., Liu, Y., Liu, H. & Tang, W. H. Exosomes: biogenesis, biologic function and clinical potential. *Cell & Bioscience* **9**, 19 (2019).

111. Sahu, R. *et al.* Microautophagy of cytosolic proteins by late endosomes. *Dev Cell* **20**, 131–139 (2011).

112. Zhang, Y., Liu, Y., Liu, H. & Tang, W. H. Exosomes: biogenesis, biologic function and clinical potential. *Cell & Bioscience* **9**, 19 (2019).

113. Xie, S., Zhang, Q. & Jiang, L. Current Knowledge on Exosome Biogenesis, Cargo-Sorting Mechanism and Therapeutic Implications. *Membranes* **12**, 498 (2022).

114. Perez-Hernandez, D. *et al.* The intracellular interactome of tetraspanin-enriched microdomains reveals their function as sorting machineries toward exosomes. *J Biol Chem* **288**, 11649–11661 (2013).

115. Tricarico, C., Clancy, J. & D'Souza-Schorey, C. Biology and biogenesis of shed microvesicles. *Small GTPases* **8**, 220–232 (2016).

116. Jeppesen, D. K., Zhang, Q., Franklin, J. L. & Coffey, R. J. Extracellular vesicles and nanoparticles: emerging complexities. *Trends Cell Biol* **33**, 667–681 (2023).

117. Morello, M. *et al.* Large oncosomes mediate intercellular transfer of functional microRNA. *Cell Cycle* **12**, 3526–3536 (2013).

118. Minciacchi, V. R. *et al.* MYC Mediates Large Oncosome-Induced Fibroblast Reprogramming in Prostate Cancer. *Cancer Res* **77**, 2306–2317 (2017).

119. Zou, X. *et al.* Advances in biological functions and applications of apoptotic vesicles. *Cell Communication and Signaling* **21**, 260 (2023).

120. Eulalio, A., Huntzinger, E. & Izaurralde, E. Getting to the root of miRNA-mediated gene silencing. *Cell* **132**, 9–14 (2008).

121. Friedman, R. C., Farh, K. K.-H., Burge, C. B. & Bartel, D. P. Most mammalian mRNAs are conserved targets of microRNAs. *Genome Res* **19**, 92–105 (2009).

122. Devulder, J., Baker, J. R., Odqvist, L., Donnelly, L. E. & Barnes, P. J. Extracellular vesicles propagate cellular senescence by transferring miR34a in airway epithelial cells. *European Respiratory Journal* **60**, (2022).

123. Guo, Z. *et al.* Exosomal miR-214-3p from senescent osteoblasts accelerates endothelial cell senescence. *J Orthop Surg Res* **18**, 391 (2023).

124. Mrazkova, B. *et al.* Induction, regulation and roles of neural adhesion molecule L1CAM in cellular senescence. *Aging* **10**, 434–462 (2018).

125. Zhao, S. *et al.* Exosomal transfer of miR-181b-5p confers senescence-mediated doxorubicin resistance via modulating BCLAF1 in breast cancer. *Br J Cancer* **128**, 665–677 (2023).

126. Buratta, S. *et al.* Extracellular vesicles released by fibroblasts undergoing H-Ras induced senescence show changes in lipid profile. *PLOS ONE* **12**, e0188840 (2017).

127. Głuchowska, A. *et al.* Unbiased proteomic analysis of extracellular vesicles secreted by senescent human vascular smooth muscle cells reveals their ability to modulate immune cell functions. *GeroScience* **44**, 2863–2884 (2022).

128. Hanley, S., Chen, Y.-Y., Hazeldine, J. & Lord, J. M. Senescent cell-derived extracellular vesicles as potential mediators of innate immunosenescence and inflammaging. *Experimental Gerontology* **187**, 112365 (2024).

129. The UniProt Consortium. UniProt: the Universal Protein Knowledgebase in 2023. *Nucleic Acids Research* **51**, D523–D531 (2023).

130. Comprehensive Overview of Bottom-Up Proteomics Using Mass Spectrometry | ACS Measurement Science Au. https://pubs.acs.org/doi/10.1021/acsmeasuresciau.3c00068.

131. Hughes, C. S. *et al.* Single-pot, solid-phase-enhanced sample preparation for proteomics experiments. *Nat Protoc* **14**, 68–85 (2019).

132. Hughes, C. S. *et al.* Ultrasensitive proteome analysis using paramagnetic bead technology. *Molecular Systems Biology* **10**, 757 (2014).

133. Kassem, S. *et al.* Proteomics for Low Cell Numbers: How to Optimize the Sample Preparation Workflow for Mass Spectrometry Analysis. *J. Proteome Res.* **20**, 4217–4230 (2021).

134. Suelter, C. H. & DeLuca, M. How to prevent losses of protein by adsorption to glass and plastic. *Anal Biochem* **135**, 112–119 (1983).

135. Yu, F., Haynes, S. E. & Nesvizhskii, A. I. IonQuant Enables Accurate and Sensitive Label-Free Quantification With FDR-Controlled Match-Between-Runs. *Mol Cell Proteomics* **20**, 100077 (2021).

136. Chambers, M. C. *et al.* A cross-platform toolkit for mass spectrometry and proteomics. *Nat Biotechnol* **30**, 918–920 (2012).

137. Yu, F. *et al.* Analysis of DIA proteomics data using MSFragger-DIA and FragPipe computational platform. *Nat Commun* **14**, 4154 (2023).

138. Tyanova, S. *et al.* The Perseus computational platform for comprehensive analysis of (prote)omics data. *Nat Methods* **13**, 731–740 (2016).

139. Hsiao, Y. *et al.* Analysis and Visualization of Quantitative Proteomics Data Using FragPipe-Analyst. *J. Proteome Res.* **23**, 4303–4315 (2024).

140. MacLean, B. *et al.* Skyline: an open source document editor for creating and analyzing targeted proteomics experiments. *Bioinformatics* **26**, 966–968 (2010).

141. Doncheva, N. T., Morris, J. H., Gorodkin, J. & Jensen, L. J. Cytoscape StringApp: Network Analysis and Visualization of Proteomics Data. *J Proteome Res* **18**, 623–632 (2019).

142. Shannon, P. *et al.* Cytoscape: a software environment for integrated models of biomolecular interaction networks. *Genome Res* **13**, 2498–2504 (2003).

143. Kues, W. A. *et al.* Cell Cycle Synchronization of Porcine Fetal Fibroblasts: Effects of Serum Deprivation and Reversible Cell Cycle Inhibitors1. *Biology of Reproduction* **62**, 412–419 (2000).

144. Wheaton, K. *et al.* Progerin-Induced Replication Stress Facilitates Premature Senescence in Hutchinson-Gilford Progeria Syndrome. *Mol Cell Biol* **37**, e00659-16 (2017).

145. Higuchi, A., Shimmura, S., Takeuchi, T., Suematsu, M. & Tsubota, K. Elucidation of apoptosis induced by serum deprivation in cultured conjunctival epithelial cells. *Br J Ophthalmol* **90**, 760–764 (2006).

146. Zhang, J. *et al.* A Human iPSC Model of Hutchinson Gilford Progeria Reveals Vascular Smooth Muscle and Mesenchymal Stem Cell Defects. *Cell Stem Cell* **8**, 31–45 (2011).

147. Chen, Z. *et al.* Reprogramming progeria fibroblasts re-establishes a normal epigenetic landscape. *Aging Cell* **16**, 870–887 (2017).

148. Urzì, O., Olofsson Bagge, R. & Crescitelli, R. The dark side of foetal bovine serum in extracellular vesicle studies. *J Extracell Vesicles* **11**, e12271 (2022).

149. Tang, Y., Zhou, Y. & Li, H.-J. Advances in mesenchymal stem cell exosomes: a review. *Stem Cell Res Ther* **12**, 71 (2021).

150. Urzì, O. *et al.* Heat inactivation of foetal bovine serum performed after EV-depletion influences the proteome of cell-derived extracellular vesicles. *Journal of Extracellular Vesicles* **13**, e12408 (2024).

151. György, B. *et al.* Detection and isolation of cell-derived microparticles are compromised by protein complexes resulting from shared biophysical parameters. *Blood* **117**, e39–e48 (2011).

152. Osteikoetxea, X. *et al.* Differential detergent sensitivity of extracellular vesicle subpopulations. *Org Biomol Chem* **13**, 9775–9782 (2015).

153. Nonnis, S. *et al.* Effect of fetal bovine serum in culture media on MS analysis of mesenchymal stromal cells secretome. *EuPA Open Proteomics* **10**, 28–30 (2016).

154. Mannerström, B. *et al.* Extracellular small non-coding RNA contaminants in fetal bovine serum and serum-free media. *Sci Rep* **9**, 5538 (2019).

155. Théry, C., Amigorena, S., Raposo, G. & Clayton, A. Isolation and characterization of exosomes from cell culture supernatants and biological fluids. *Curr Protoc Cell Biol* **Chapter 3**, Unit 3.22 (2006).

156. Li, K., Wong, D. K., Hong, K. Y. & Raffai, R. L. Cushioned–Density Gradient Ultracentrifugation (C–DGUC): a Refined and High Performance Method for the Isolation, Characterization & Use of Exosomes. *Methods Mol Biol* **1740**, 69–83 (2018).

157. Zhang, H. *et al.* Identification of distinct nanoparticles and subsets of extracellular vesicles by asymmetric-flow field-flow fractionation. *Nat Cell Biol* **20**, 332–343 (2018).

158. Zhang, Q. *et al.* Supermeres are functional extracellular nanoparticles replete with disease biomarkers and therapeutic targets. *Nat Cell Biol* **23**, 1240–1254 (2021).

159. Peterson, A. C., Russell, J. D., Bailey, D. J., Westphall, M. S. & Coon, J. J. Parallel reaction monitoring for high resolution and high mass accuracy quantitative, targeted proteomics. *Mol Cell Proteomics* **11**, 1475–1488 (2012).

160. Kong, A. T., Leprevost, F. V., Avtonomov, D. M., Mellacheruvu, D. & Nesvizhskii, A. I. MSFragger: ultrafast and comprehensive peptide identification in mass spectrometry–based proteomics. *Nat Methods* **14**, 513–520 (2017).

161. Kong, W., Hui, H. W. H., Peng, H. & Goh, W. W. B. Dealing with missing values in proteomics data. *PROTEOMICS* **22**, 2200092 (2022).

162. Yu, F., Haynes, S. E. & Nesvizhskii, A. I. IonQuant Enables Accurate and Sensitive Label-Free Quantification With FDR-Controlled Match-Between-Runs. *Molecular & Cellular Proteomics* **20**, 100077 (2021).

163. San Martin, R., Das, P., Sanders, J. T., Hill, A. M. & McCord, R. P. Transcriptional profiling of Hutchinson-Gilford Progeria syndrome fibroblasts reveals deficits in mesenchymal stem cell commitment to differentiation related to early events in endochondral ossification. *eLife* **11**, e81290 (2022).

164. Rivera-Torres, J. *et al.* Identification of mitochondrial dysfunction in Hutchinson–Gilford progeria syndrome through use of stable isotope labeling with amino acids in cell culture. *Journal of Proteomics* **91**, 466–477 (2013).

165. Graziotto, J. J., Cao, K., Collins, F. S. & Krainc, D. Rapamycin activates autophagy in Hutchinson-Gilford progeria syndrome. *Autophagy* **8**, 147–151 (2012).

166. Yi, L. *et al.* NTN4 as a prognostic marker and a hallmark for immune infiltration in breast cancer. *Sci Rep* **12**, 10567 (2022).

167. Tanaka, I. *et al.* SRGN-Triggered Aggressive and Immunosuppressive Phenotype in a Subset of TTF-1–Negative Lung Adenocarcinomas. *J Natl Cancer Inst* **114**, 290–301 (2021).

168. Qian, Y. *et al.* SRGN amplifies microglia-mediated neuroinflammation and exacerbates ischemic brain injury. *Journal of Neuroinflammation* **21**, 35 (2024).

169. Jendoubi, T. Approaches to Integrating Metabolomics and Multi-Omics Data: A Primer. *Metabolites* **11**, 184 (2021).

170. Reyes, R., Cardeñes, B., Machado-Pineda, Y. & Cabañas, C. Tetraspanin CD9: A Key Regulator of Cell Adhesion in the Immune System. *Front. Immunol.* **9**, (2018).

171. Marin, I. *et al.* Cellular Senescence Is Immunogenic and Promotes Antitumor Immunity. *Cancer Discovery* **13**, 410–431 (2023).

172. Chen, H.-A. *et al.* Senescence Rewires Microenvironment Sensing to Facilitate Antitumor Immunity. *Cancer Discovery* **13**, 432–453 (2023).

173. Fernández-Messina, L. *et al.* Transfer of extracellular vesicle-microRNA controls germinal center reaction and antibody production. *EMBO Rep* **21**, e48925 (2020).

174. Han, P. *et al.* 3D bioprinted small extracellular vesicles from periodontal cells enhance mesenchymal stromal cell function. *Biomaterials Advances* **158**, 213770 (2024).

175. Li, J., He, X., Deng, Y. & Yang, C. An Update on Isolation Methods for Proteomic Studies of Extracellular Vesicles in Biofluids. *Molecules* **24**, 3516 (2019).

176. Torres, A. *et al.* Comparing the Proteomic Profiles of Extracellular Vesicles Isolated using Different Methods from Long-term Stored Plasma Samples. *Biological Procedures Online* **26**, 18 (2024).

177. Reymond, S., Gruaz, L. & Sanchez, J.-C. Depletion of abundant plasma proteins for extracellular vesicle proteome characterization: benefits and pitfalls. *Anal Bioanal Chem* **415**, 3177–3187 (2023).

178. van der Pol, E. *et al.* Particle size distribution of exosomes and microvesicles determined by transmission electron microscopy, flow cytometry, nanoparticle tracking analysis, and resistive pulse sensing. *J Thromb Haemost* **12**, 1182–1192 (2014).

179. Tian, Y. *et al.* Quality and efficiency assessment of six extracellular vesicle isolation methods by nano-flow cytometry. *J Extracell Vesicles* **9**, 1697028 (2020).

180. Zhang, H. & Lyden, D. Asymmetric flow field-flow fractionation technology for exomere and small extracellular vesicle separation and characterization. *Nat Protoc* **14**, 1027–1053 (2019).

181. Bayart, C. *et al.* Comparison of SEC and AF4 analytical tools for size estimation of typhoid Vi polysaccharides. *Anal. Methods* **11**, 4851–4858 (2019).

182. Benedikter, B. J. *et al.* Ultrafiltration combined with size exclusion chromatography efficiently isolates extracellular vesicles from cell culture media for compositional and functional studies. *Sci Rep* **7**, 15297 (2017).

183. Franco, C. *et al.* Size-Exclusion Chromatography Combined with Ultrafiltration Efficiently Isolates Extracellular Vesicles from Human Blood Samples in Health and Disease. *Int J Mol Sci* **24**, 3663 (2023).

184. Huang, B. X., Kim, H.-Y. & Dass, C. Probing three-dimensional structure of bovine serum albumin by chemical cross-linking and mass spectrometry. *J Am Soc Mass Spectrom* **15**, 1237–1247 (2004).

185. Rath, S. *et al.* MitoCarta3.0: an updated mitochondrial proteome now with sub-organelle localization and pathway annotations. *Nucleic Acids Res* **49**, D1541–D1547 (2021).

186. Picca, A. *et al.* Mitochondrial-Derived Vesicles: The Good, the Bad, and the Ugly. *Int J Mol Sci* **24**, 13835 (2023).

187. Gordon, L. B. *et al.* Plasma Progerin in Patients With Hutchinson-Gilford Progeria Syndrome: Immunoassay Development and Clinical Evaluation. *Circulation* **147**, 1734–1744 (2023).

188. Uhlén, M. *et al.* Tissue-based map of the human proteome. *Science* **347**, 1260419 (2015).

189. Zhang, H., Xiong, Z.-M. & Cao, K. Mechanisms controlling the smooth muscle cell death in progeria via down-regulation of poly(ADP-ribose) polymerase 1. *Proc Natl Acad Sci U S A* **111**, E2261–E2270 (2014).

190. Fitzgerald, W. *et al.* A System of Cytokines Encapsulated in ExtraCellular Vesicles. *Sci Rep* **8**, 8973 (2018).

191. Adiko, A. C., Babdor, J., Gutiérrez-Martínez, E., Guermonprez, P. & Saveanu, L. Intracellular Transport Routes for MHC I and Their Relevance for Antigen Cross-Presentation. *Front Immunol* **6**, 335 (2015).

192. Cheng, H. *et al.* Identification of a Missense Variant in LNPEP that Confers Psoriasis Risk. *Journal of Investigative Dermatology* **134**, 359–365 (2014).

193. Paladini, F., Fiorillo, M. T., Tedeschi, V., Mattorre, B. & Sorrentino, R. The Multifaceted Nature of Aminopeptidases ERAP1, ERAP2, and LNPEP: From Evolution to Disease. *Front. Immunol.* **11**, (2020).

194. Hawkins, N. J., Ward, R. L. & Wakefield, D. Cytokine-mediated induction of HLA antigen expression on human glomerular mesangial cells. *Cell Immunol* **155**, 493–500 (1994).

195. Johansson, T., Partanen, J. & Saavalainen, P. HLA allele-specific expression: Methods, disease associations, and relevance in hematopoietic stem cell transplantation. *Front Immunol* **13**, 1007425 (2022).

196. Petersdorf, E. W. *et al.* HLA-C expression levels define permissible mismatches in hematopoietic cell transplantation. *Blood* **124**, 3996–4003 (2014).

197. Xia, P., Shao, Y.-Q., Yu, C.-C., Xie, Y. & Zhou, Z.-J. NLRP3 inflammasome up-regulates major histocompatibility complex class I expression and promotes inflammatory infiltration in polymyositis. *BMC Immunology* **23**, 39 (2022).

198. Coll-Bonfill, N., Cancado de Faria, R., Bhoopatiraju, S. & Gonzalo, S. Calcitriol Prevents RAD51 Loss and cGAS-STING-IFN Response Triggered by Progerin. *Proteomics* **20**, e1800406 (2020).

199. Yi, Y. *et al.* Mesenchymal Stromal Cells Increase the Natural Killer Resistance of Circulating Tumor Cells via Intercellular Signaling of cGAS-STING-IFNβ-HLA. *Advanced Science* **11**, 2400888 (2024).

200. Blest, H. T. W. & Chauveau, L. cGAMP the travelling messenger. *Front Immunol* **14**, 1150705 (2023).

201. Fafián-Labora, J. A., Rodríguez-Navarro, J. A. & O'Loghlen, A. Small Extracellular Vesicles Have GST Activity and Ameliorate Senescence-Related Tissue Damage. *Cell Metab* **32**, 71-86.e5 (2020).

202. Allegra, S., Chiara, F., Di Grazia, D., Gaspari, M. & De Francia, S. Evaluation of Sex Differences in Preclinical Pharmacology Research: How Far Is Left to Go? *Pharmaceuticals* **16**, 786 (2023).

203. Justice, M. J. Sex matters in preclinical research. *Dis Model Mech* **17**, dmm050759 (2024).

204. Noren Hooten, N., Byappanahalli, A. M., Vannoy, M., Omoniyi, V. & Evans, M. K. Influences of age, race, and sex on extracellular vesicle characteristics. *Theranostics* **12**, 4459–4476 (2022).

205. Bammert, T. D. *et al.* Influence of sex on the number of circulating endothelial microparticles and microRNA expression in middle-aged adults. *Exp Physiol* **102**, 894–900 (2017).

206. Penaloza, C. *et al.* Sex of the cell dictates its response: differential gene expression and sensitivity to cell death inducing stress in male and female cells. *FASEB J* **23**, 1869–1879 (2009).

207. Weber, C. M. & Clyne, A. M. Sex differences in the blood–brain barrier and neurodegenerative diseases. *APL Bioengineering* **5**, 011509 (2021).

208. SAGD: a comprehensive sex-associated gene database from transcriptomes | Nucleic Acids Research | Oxford Academic. https://academic.oup.com/nar/article/47/D1/D835/5150230.

209. Yang, M. *et al.* SexAnnoDB, a knowledgebase of sex-specific regulations from multi-omics data of human cancers. *Biology of Sex Differences* **15**, 64 (2024).

210. Zhao, L.-F. *et al.* SDC: An integrated database for sex differences in cancer. *Computational and Structural Biotechnology Journal* **20**, 1068–1076 (2022).

211. Soekmadji, C. *et al.* The future of Extracellular Vesicles as Theranostics – an ISEV meeting report. *J Extracell Vesicles* **9**, 1809766 (2020).

212. Shah, K., McCormack, C. E. & Bradbury, N. A. Do you know the sex of your cells? *American Journal of Physiology-Cell Physiology* **306**, C3–C18 (2014).

213. Noren Hooten, N. *et al.* Association of Extracellular Vesicle Protein Cargo with Race and Clinical Markers of Mortality. *Sci Rep* **9**, 17582 (2019).

214. Hennekam, R. C. M. Hutchinson–Gilford progeria syndrome: Review of the phenotype. *American Journal of Medical Genetics Part A* **140A**, 2603–2624 (2006).

215. Fernández-Costa, C. *et al.* Impact of the identification strategy on the reproducibility of DDA and DIA results. *J Proteome Res* **19**, 3153–3161 (2020).

216. Yang, Y. *et al.* In silico spectral libraries by deep learning facilitate data-independent acquisition proteomics. *Nat Commun* **11**, 146 (2020).

217. Isaksson, M., Karlsson, C., Laurell, T., Kirkeby, A. & Heusel, M. MSLibrarian: Optimized Predicted Spectral Libraries for Data-Independent Acquisition Proteomics. *J Proteome Res* **21**, 535–546 (2022).

218. Tremblay, T.-L., Fauteux, F., Callaghan, D. & Hill, J. J. Cell surface profiling of cultured cells by direct hydrazide capture of oxidized glycoproteins. *MethodsX* **11**, 102349 (2023).

219. Kaur, G. *et al.* Structural and regulatory diversity shape HLA-C protein expression levels. *Nat Commun* **8**, 15924 (2017).

220. CORD, C. O. for R. D. Now if the Time: A Strategy for Rare Diseases is a Strategy for All Canadians. (2015).

221. Mosevitsky, M. I. Progerin and Its Role in Accelerated and Natural Aging. *Mol Biol* **56**, 125–146 (2022).

222. Benedikter, B. J. *et al.* Ultrafiltration combined with size exclusion chromatography efficiently isolates extracellular vesicles from cell culture media for compositional and functional studies. *Sci Rep* **7**, 15297 (2017).

8. APPENDIX

Supplemental Table 1: R Packages Used

R Package	Version	Use case
dplyr	1.1.4	Data filtering and manipulation
ggrepel	0.9.6	Graphing
ggplot2	3.5.1	Graphing

Supplemental Table 2: The proteome of EV-free FBS.

Proteins are ordered by decreasing proportion of LFQ total abundance, averaged across 3 mass spectrometric technical replicates. Protein with "-" proportion of intensity contributed less than 0.01% of total observed intensity, therefore the sum of the proportions is less than 100%.

Protein Name	Proportion of LFQ Intensity	Protein Name	Proportion of LFQ Intensity	Protein Name	Proportion of LFQ Intensity	Protein Name	Proportion of LFQ Intensity	Protein Name	Proportion of LFQ Intensity	Protein Name	Proportion of LFQ Intensity
ALB	32.29%	ITIH4	0.75%	IPLA	0.29%	ACT18	-	F10	-	MST1	-
AHSG	10.81%	ITIH2	0.67%	CFH	0.29%	ACTBL2	-	F12	-	MT1B	-
GSN	7.78%	KNG2	0.66%	ORM1	0.26%	AF_1514	-	F5	-	MYO1C	-
TF	5.69%	SERPINA3-1	0.62%	ADIPOQ	0.24%	APOB	-	F9	-	PFN1	-
GC	4.19%	PLG	0.60%	FGA	0.24%	APOC3	-	FBLN1	-	POSTN	-
AFP	3.31%	APOH	0.57%	APOA4	0.24%	APOD	-	FLA10	-	PROC	-
C3	2.22%	VNN1	0.57%	FN1	0.23%	BDG2	-	HABP2	-	PROS1	-
SERPINF1	2.04%	RPOC1	0.55%	F2	0.22%	BDP1	-	HGFAC	-	PZP	-
SLC47A1	1.77%	ITIH3	0.53%	AFM	0.22%	C4A	-	HRG	-	RBP4	-
SERPINA6	1.61%	CFB	0.52%	APOA2	0.21%	CDH5	-	IGF2	-	SHBG	-
A1BG	1.58%	SERPINF2	0.52%	AMBP	0.21%	CDK12	-	IGFBP4	-	SRP54	-
APOA1	1.54%	AGT	0.52%	SERPINA7	0.21%	CFD	-	ITIH1	-	TCDA	-
A2M	1.26%	FAM186A	0.45%	IGFBP2	0.20%	CL43	-	KLKB1	-	THBS1	-
PF4	1.25%	SERPINA3-3	0.42%	ACTB	0.19%	COL1A1	-	KRT10	-	THBS4	-
SERPINA1	1.24%	CLEC3B	0.38%	SERPINA3-7	0.18%	COL1A2	-	KRT2	-	TTR	-
SERPINA5	1.02%	HBB	0.35%	HPX	0.16%	COL2A1	-	KRT6A	-	VCL	-
KNG1	0.99%	INHCA	0.35%	C7	0.14%	COL3A1	-	KRT75	-	VWF	-
SERPINC1	0.94%	LTF	0.34%	CLU	0.14%	COL6A1	-	LUM	-		
FETUB	0.83%	SERPINA3-8	0.31%	SERPINA3-5	0.14%	COMP	-	MB	-		
HBA	0.83%	C4	0.31%	ACT3	0.14%	CPB2	-	METK	-		
C9	0.80%	APOE	0.30%	SERPINA3-6	0.13%	CYIIIB	-	MSH1	-		

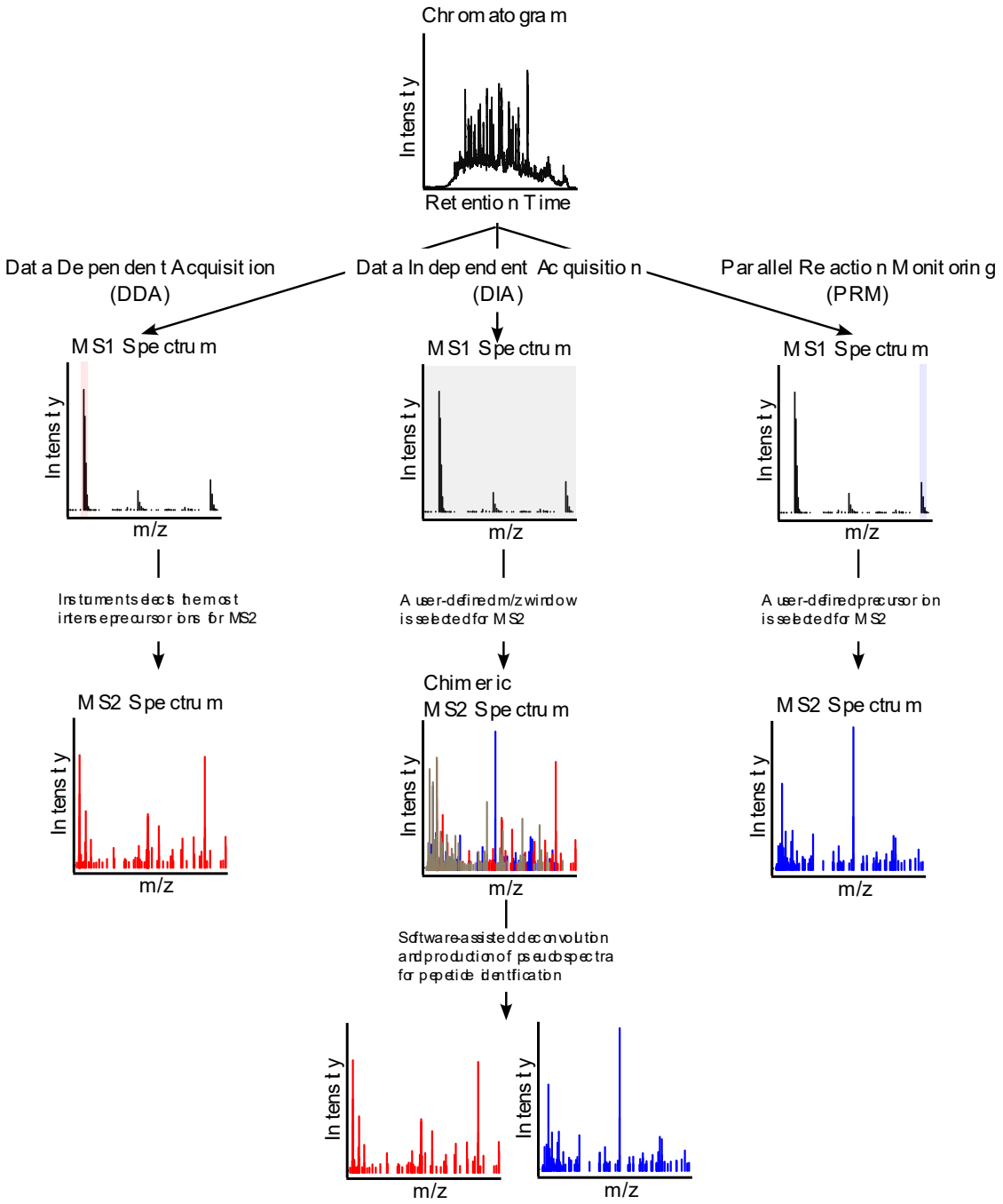

Supplemental Figure 1: Comparing acquisition methods in mass spectrometry.

In data dependent mass (DDA) spectrometry, only the top N most abundant precursor ions (peptides with a specific charge) from MS1 are selected for fragmentation and subsequent MS2 acquisition. In contrast, data independent acquisition (DIA) methods cycle through pre-defined windows of the MS1 spectrum containing many precursor ions for fragmentation and subsequent MS2 acquisition, theoretically, acquiring fragment ions for all precursors regardless of their relative intensity during MS1. Therefore, DIA should contain much more fragment-level data and may be better to quantify low abundant proteins. Parallel reaction monitoring (PRM) uses user-defined precursor ions in the MS1 scan to acquire MS2 scans, regardless of relative intensity to other ions in the MS1 scan.

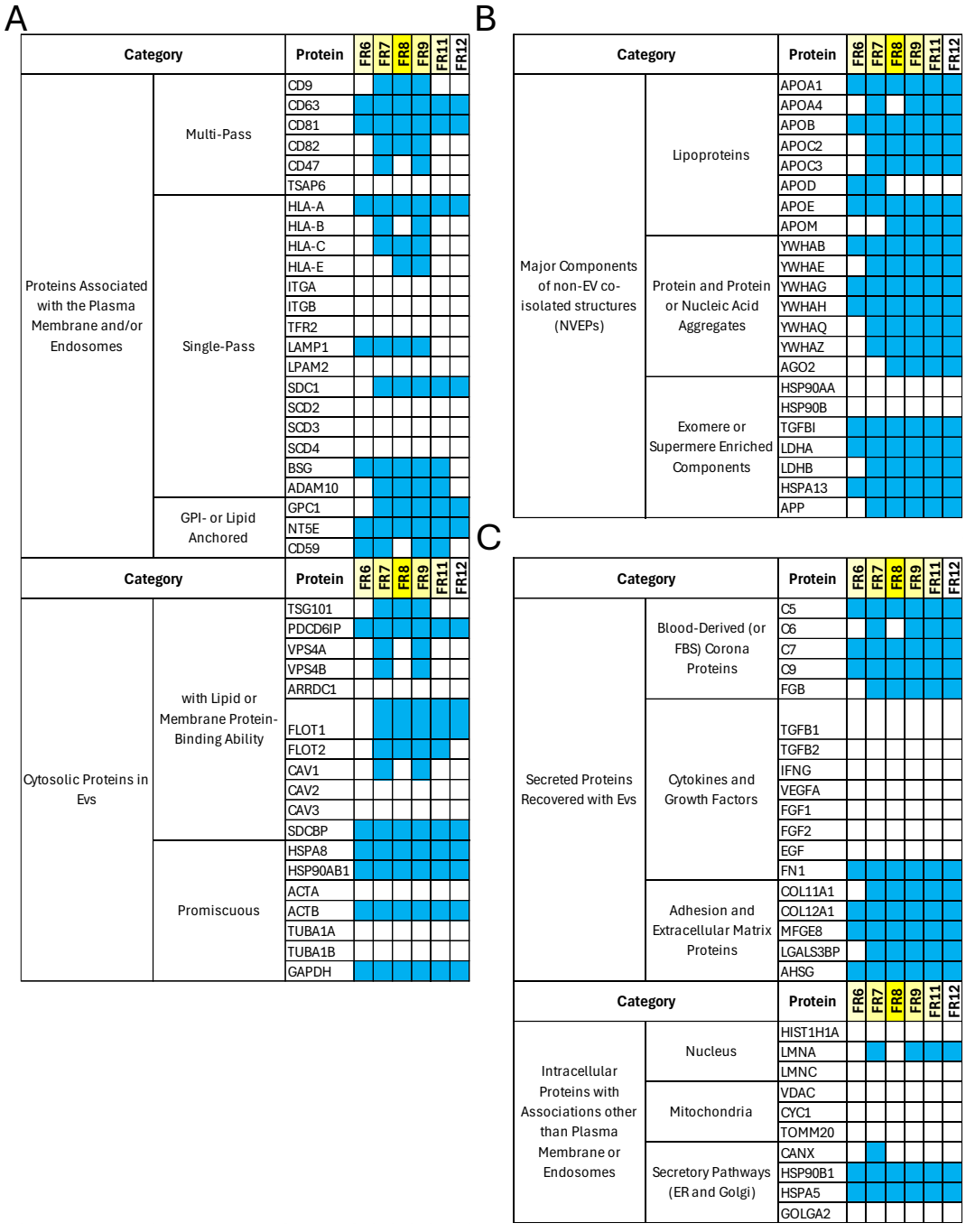

Supplemental Figure 2: List of EV-associated proteins used for EV characterization.

(A) Proteins strongly associated with EVs, which are oftentimes used as EV markers. **(B)** Proteins associated with other structures which are oftentimes co-isolated with EVs, such as NVEPs. **(C)** Proteins which are secreted but may be associated with EVs. The lists presented are non-exhaustive and serve as a recommended standard framework for reporting EV content[107]. Blue squares represent the protein was identified in this fraction.

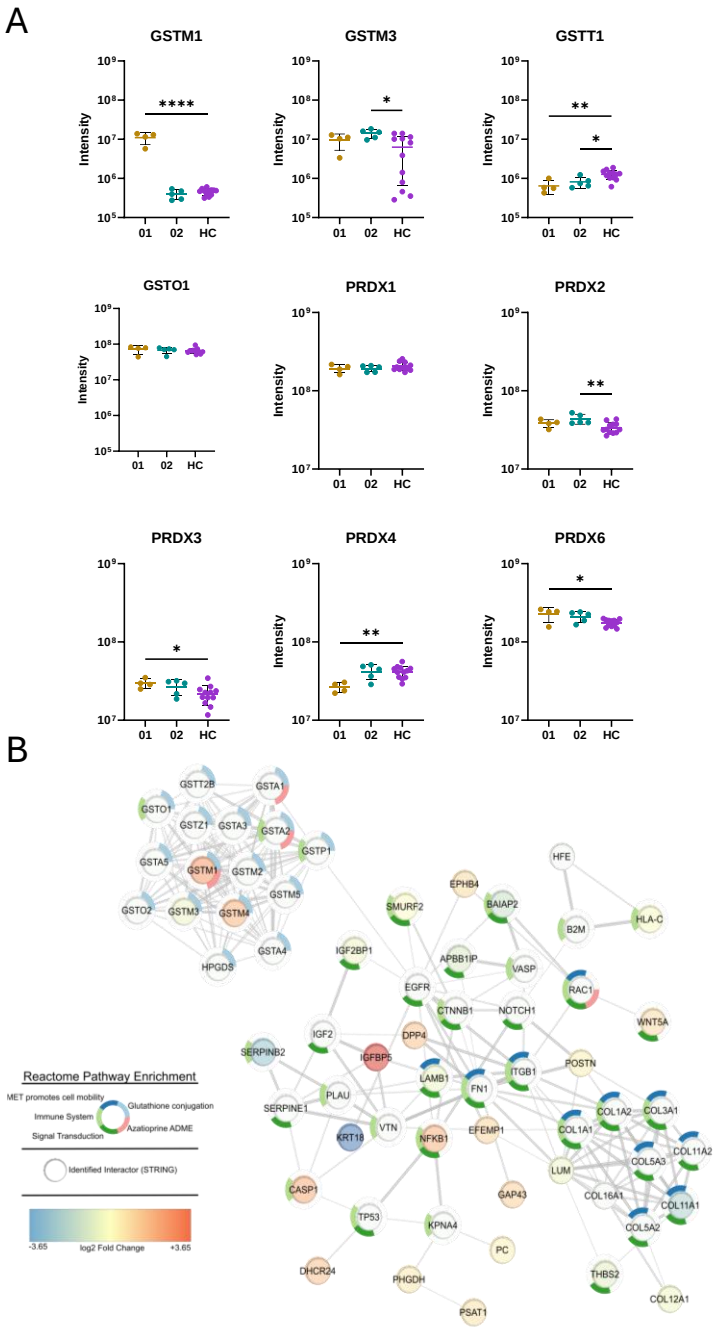

Supplemental Figure 3: Dysregulation of glutathione metabolism

(A) Various glutathione-S transferases (GST) were quantified using LC-MS/MS. Mu GSTs were mildly upregulated in HGPS WCL. Dysregulation in peroxiredoxins was also observed in HGPS-01. * p<0.05, ** p<0.01, ***p<0.001. **(B)** Differentially expressed protein in HGPS WCL (Figure 8) were imported into Cytoscape for visualization and subsequently searched for physical PPIs (protein-protein interactions) with the STRING database using a confidence score of 0.4, while allowing for network expansion of 50% (33 protein). The largest subnetwork was exported for enrichment analysis against the Reactome database. Fold change calculated as Healthy/HGPS. Blue is higher in HGPS.